KAMAN AVIDYNE TR-55

A TERMINAL GUIDANCE SCHEME FOR LIFTING BODY ENTRY VEHICLES

by William C. Hoffman, Arthur E. Bryson, Jr., *and* John Zvara

OCTOBER 1968

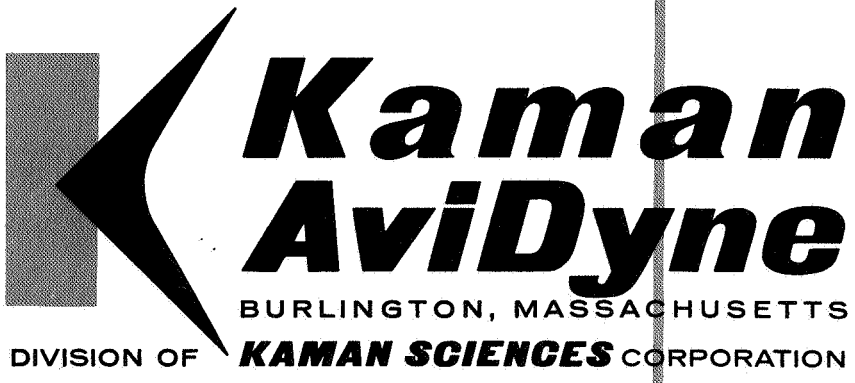

prepared for
Electronics Research Center
NATIONAL AERONAUTICS AND SPACE ADMINISTRATION

ERRATA

Kaman AviDyne TR-55

A Terminal Guidance Scheme for Lifting Body Entry Vehicles

Page i	Replace "FOREWARD" with "FOREWORD
Page v	Insert under Section II: "2.5 Summary ... 22"
Page xiii	Definition of σ_γ should read: "Standard deviation in flight path angle error"
Page xiii	Definition of σ_ψ should read: "Standard deviation in heading angle error"
Page 36	Fourth and third lines from bottom should read: "... for initial crossrange errors of ±5000 m, and for initial heading errors of ±50°"
Page 77	Title of Reference 7 should read: "Six-Degree of Freedom Analysis of Lifting Entry Vehicle..."
Page 78	Publication date of Reference 15 should be 1969

KAMAN AVIDYNE
a Division of Kaman Sciences Corporation
Burlington, Massachusetts

KAMAN AVIDYNE TR-55

A TERMINAL GUIDANCE SCHEME FOR LIFTING BODY ENTRY VEHICLES

by

William C. Hoffman, Arthur E. Bryson, Jr.,
and John Zvara

October 1968

Prepared under Contract No. NAS 12-99
for the Electronics Research Center
NATIONAL AERONAUTICS AND SPACE ADMINISTRATION

FOREWARD

This report was prepared by the Kaman AviDyne Division of Kaman Sciences Corporation, Burlington, Massachusetts. It presents the final documentation of the effort conducted for the NASA Electronics Research Center, Cambridge, Massachusetts, under Modification 2 of Contract NAS 12-99. The work covered in this report was performed in the period from October 1967 through September 1968. The contract was monitored for the National Aeronautics and Space Administration by Miss Ann Muzyka.

The work was performed under the direction of Dr. N. P. Hobbs, General Manager of Kaman AviDyne. Mr. John Zvara acted as Program Manager, and Mr. William C. Hoffman served as Project Leader and Principal Investigator. Prof. A. E. Bryson of Stanford University was Technical Consultant for the study. Miss Linda K. Serfilippi and Miss Kathleen A. McKeon provided invaluable assistance in obtaining the numerical results.

ABSTRACT

A simple perturbation feedback scheme is developed for guiding a lifting body entry vehicle during the terminal phase of flight. By observing that the velocity and flight path angle of typical lifting body vehicles become quasi-steady during subsonic flight, and by selecting altitude rather than time as the independent variable, one can reduce the number of state variables to three. The system may then be linearized by taking first-order perturbations about a nominal trajectory. An effective linear feedback guidance law is obtained by selecting a performance index which is quadratic in both the state and the control variables. The minimization of this performance index leads to a third-order matrix Ricatti equation, the solution of which yields the optimal feedback gains.

To implement the terminal guidance scheme, the nominal state variables, the nominal control variables, and the feedback gains are pre-calculated and stored as functions of altitude in the onboard computer. During flight, the actual state variables are measured and their deviations from nominal are used to calculate optimal corrections to the stored nominal control variables.

Numerical results are presented for a typical vehicle performing both a straight-in approach and a 90^{o} turn followed by a straight glide. These results indicate that the scheme can successfully handle a variety of off-nominal conditions. The effects of initial condition errors, winds, atmospheric density variations, and uncertainties in the vehicle characteristics are included.

TABLE OF CONTENTS

LIST OF ILLUSTRATIONS

LIST OF ILLUSTRATIONS (CONT'D)

LIST OF TABLES

GLOSSARY OF SYMBOLS

Symbol	Units	Definition
g	m/sec^2	Acceleration of gravity (9.80 m/sec^2)
h	m	Altitude above sea level; defined by Equation (39)
h_R	m	Altitude of runway above sea level
ℓ	m	Characteristic length of vehicle; defined by $\ell = \frac{2 m \eta}{\rho C_{L_\alpha} S_{ref}}$
m	kg	Mass of vehicle
$\bar{u}$	—	Control vector of simplified system; defined by Equation (27)
w_x	m/sec	Wind velocity in x-direction
w_y	m/sec	Wind velocity in y-direction
x	m	Downrange position coordinate; see Figure 2
$\bar{x}$	—	3 x 1 state vector of linearized simplified system; defined by Equation (26)
y	m	Crossrange position coordinate; see Figure 2
$\bar{y}$	—	5 x 1 state vector of linearized system; defined by Equation (41)
z	m	Vertical position coordinate; see Figure 2
A	—	3 x 3 penalty matrix on en route state variable deviations; see Equations (30) and (32)
B	—	2 x 2 penality matrix on control deviations; see Equations (30) and (33)
C	—	2 x 3 matrix of guidance feedback gains, defined by Equation (35)
C_{D_o}	—	Aerodynamic drag coefficient for zero lift

Symbol	Units	Definition
C_{L_α}	deg^{-1}	Aerodynamic lift curve slope; defined by $C_{L_\alpha} = \frac{2}{\rho V^2 S_{ref}} \frac{\partial L}{\partial \alpha}$
$C_{\alpha x}$	deg/m	Feedback gain for α due to error in x; see Equation (38)
$C_{\alpha y}$	deg/m	Feedback gain for α due to error in y; see Equation (38)
$C_{\alpha \psi}$	deg/deg	Feedback gain for α due to error in ψ; see Equation (38)
$C_{\phi x}$	deg/m	Feedback gain for ϕ due to error in x; see Equation (38)
$C_{\phi y}$	deg/m	Feedback gain for ϕ due to error in y; see Equation (38)
$C_{\phi \psi}$	deg/deg	Feedback gain for ϕ due to error in ψ; see Equation (38)
D	N	Aerodynamic drag force; approximated by Equation (15)
E[ ]	same as [ ]	Expected value of indicated quantity; see Equation (42)
F	—	3 x 3 homogeneous matrix of linearized simplified system; defined by Equations (25) and (28)
G	—	3 x 2 forcing matrix of linearized simplified system; defined by Equations (25) and (29)
J	—	Performance index; defined by Equation (30)
L	N	Aerodynamic lift force; approximated by Equation (14)
R	m	Local radius of helix for quasi-steady glide; defined by Equation (10)
S	—	3 x 3 Riccati matrix; defined by Equations (36) and (37)

Symbol	Units	Definition
S_f	—	3 x 3 penalty matrix on terminal state variable deviations; see Equations (30) and (31)
S_{ref}	m^2	Aerodynamic reference area of vehicle
V	m/sec	Velocity of vehicle; see Figure 2
α	deg	Angle of attack; see Figure 2
α_o	deg	Angle of attack for zero lift; see Equation (14)
$\bar{\alpha}$	—	Modified angle of attack; defined by $\bar{\alpha} = \eta(\alpha - \alpha_o)$
δ	—	Minimum drag/lift ratio of vehicle; defined by $\delta = 2\sqrt{\frac{\eta C_{D_o}}{C_{L_\alpha}}}$
$\delta( )$	same as $( )$	Perturbation in quantity indicated; defined by $\delta( ) = ( ) - ( )_N$
η	deg^{-1}	Aerodynamic efficiency factor ($0 \leq \eta \leq 1$); see Equation (15)
ρ	kg/m^3	Atmospheric density
σ_x	m	Standard deviation in downrange position error
σ_y	m	Standard deviation in crossrange position error
σ_V	m/sec	Standard deviation in velocity error
σ_γ	deg	Standard deviation in flight path angle
σ_ψ	deg	Standard deviation in heading angle
ϕ	deg	Bank angle; see Figure 2
ψ	deg	Heading angle; see Figure 2
Φ	—	Transition matrix of linearized system; see Equation (40)

SECTION I

INTRODUCTION

1.1 BACKGROUND

Lifting body entry vehicle configurations which are capable of controlled atmospheric flight and horizontal landing are under investigation for a number of future space mission applications by both NASA and the Air Force. These missions include logistic support for second generation space stations (e.g., resupply, crew rotation, rescue and emergency return), recovery of reusable boost vehicle stages, military reconnaissance, and satellite inspection or repair.

The advantage of lifting body vehicles for these advanced missions lies in their ability to maneuver to and land at one of several possible sites on a routine basis. However, certain of these missions (emergency return, for example) will require the vital capability of landing at night or under marginal weather conditions. To accomplish such landings without propulsion and with maximum lift-to-drag ratios of about three, these vehicles will require very precise terminal guidance.

For the purpose of discussing the guidance of lifting entry vehicles, it is convenient to separate the entry into three phases: (1) the initial phase, defined as that region from the top of the sensible atmosphere to 30 kilometers; (2) the final approach phase, defined as that region between 30 kilometers and the start of the flare maneuver; and (3) the flare and touchdown phase. The effort under this study

was concerned only with the second phase, but a few remarks on all three phases are appropriate for background.

A wide variety of guidance concepts for lifting entry vehicles has been reported in the technical literature. Nearly 100 prior publications are surveyed in Reference 1, and many others have subsequently appeared (e.g., References 2 and 3). The majority of these systems are concerned with the initial phase of entry and are generally capable of delivering the vehicle to the start of the final approach phase in the vicinity of the landing site with position errors of a few kilometers (km), and with velocity errors on the order of 10 meters per second (m/sec). For daylight landings under ideal weather conditions, the X-15 and lifting body test flights have shown that the pilots, utilizing visual cues and a minimum of ground instruction, are able to reduce the position and velocity errors at the beginning of the final approach phase to several meters and to fewer than ten meters per second, respectively, at the touchdown point (References 4 and 5). However, in the case of night landings or under adverse weather conditions, a precise terminal guidance system will be necessary to bring the vehicle to the landing site with sufficient accuracy to enable the pilot to complete the flare and landing maneuvers.

A pictorial description of the terminal region of flight is shown in Figure 1. The figure illustrates two types of approach patterns which may be used by unpowered lifting vehicles,

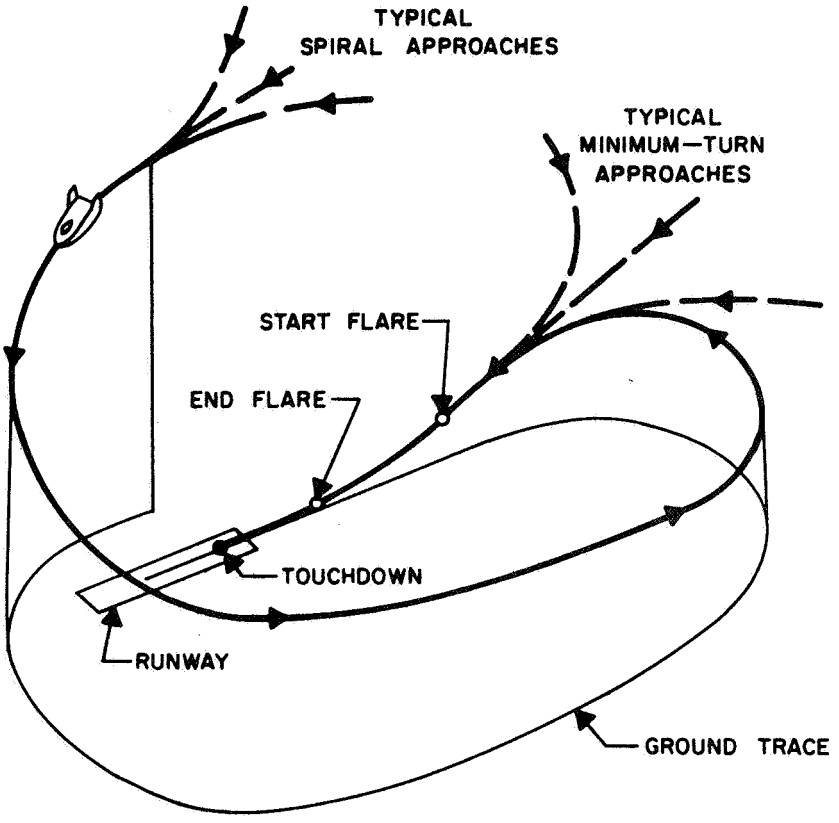

FIGURE 1. DEFINITION OF FINAL APPROACH AND FLARE MANEUVER

a minimum-turn approach and a spiral approach. A minimum-turn approach is one which uses the smallest heading change necessary to line up with the landing direction; such turns are all less than or equal to 180^{o}. A spiral approach is one which involves a turn of more than 180^{o}.

Spiral approaches were developed during the test flights of the X-series of aircraft at the NASA Flight Research Center. These approaches are preferred by pilots making visual letdowns

since they allow more opportunity to check velocity and position (by visual cues, measured data and voice communications with the ground) against a predetermined flight path. Thus, they provide wide flexibility and large error accommodation capability. The spiral pattern also requires the vehicle to approach the field at higher altitudes, enabling terminal-area ground sensors to track it at larger elevation angles. This results in improved accuracies over the low elevation tracking associated with minimum-turn approaches. However, the spiral approach does involve more maneuvering, which causes the vehicle to lose altitude slightly faster than a minimum-turn approach. Consequently, it may not be desirable for night or poor-weather landings.

The minimum-turn approach provides less flexibility and error accommodation than the spiral approach. This is of particular concern for contingency situations in which the spacecraft arrives with large excesses or deficiencies in velocity. In addition, less time is available for terminal-area ground sensors to acquire and track the vehicle, and the tracking must be performed at lower elevation angles with greater atmospheric and ground clutter effects. On the other hand, the minimum-turn approach simplifies the pilot's task and provides a slight reduction in sink rate. These are important factors during instrument letdowns under night or marginal weather conditions.

The success of the flare maneuver (also shown in Figure 1) depends largely upon the vehicle's position and velocity with respect to the runway at the start-flare point. The vehicle approaches the start-flare point in a steady-state glide aimed at a point short of the runway. The flare itself consists of a nearly constant normal acceleration maneuver which reduces the sink rate of the vehicle to an acceptable value at touchdown.

1.2 SCOPE OF INVESTIGATION

This investigation is concerned with the design of a highly accurate guidance scheme for a lifting entry vehicle in the final approach phase of flight. The current practice for the existing experimental vehicles is to limit all flight tests to daylight hours and ideal weather conditions when visual landings are possible. Obviously, such conditions will not always exist during operational missions.

Previous studies of lifting body vehicles (References 6 and 7) revealed that they approach a quasi-equilibrium glide in the terminal region of flight. By assuming such a quasi-equilibrium glide (i.e., very slow changes in velocity and flight path angle) and by using altitude rather than time as the independent variable, a simple approximation to the point-mass motions of these vehicles with only three state variables was obtained in the present study. The simplified equations were linearized about a nominal reference trajectory, and the resulting perturbation equations were used with the linear-

quadratic synthesis technique to obtain a linear feedback guidance law. The performance of this scheme was then evaluated by simulation for a variety of off-nominal conditions.

The simulation was conducted using data representative of the NASA M-2 lifting body entry vehicle. The M-2 is one of three designs which have been built for full-scale testing. The other two are the NASA HL-10 and the Air Force X-24A (formerly the SV-5) configurations. Two versions of the M-2 have been constructed and flown: the lightweight M2-F1 which was designed for low altitude, subsonic flights; and the heavier M2-F2 which was built for higher altitude flights up to supersonic speeds. More information on the M-2 lifting body program may be found in References 5 and 8 through 13.

Several simplifications have been assumed throughout this investigation to facilitate the analysis and simulation involved. The equations of motion were written for an inertial coordinate frame fixed at the touchdown point on the runway. A three degree-of-freedom, point-mass model of the vehicle was employed, and all turning maneuvers were assumed to be coordinated (i.e., no side slip). A non-rotating, flat earth was assumed since all maneuvers occur at low altitudes in the proximity of the runway, and the 1962 Standard Atmosphere (Reference 14) was used for the atmospheric density and speed of sound as functions of altitude. Furthermore, it was assumed that the vehicle's position and velocity could be measured exactly, and that the guidance commands would be

instantly and precisely obeyed by the vehicle. The investigation was limited to the subsonic flight regime to render the aerodynamic lift and drag coefficients independent of Mach number.

SECTION II

ANALYTICAL DEVELOPMENT

This section presents the analytical development of a terminal guidance scheme for lifting entry vehicles. The equations of motion are stated, approximations are introduced, and a linearization is performed about a nominal trajectory. A linear feedback guidance law is then synthesized for this simplified system.

2.1 EQUATIONS OF MOTION

The lifting body vehicle may be represented as a point mass acted upon only by aerodynamic and gravitational forces. A flat, non-rotating earth with a still atmosphere is assumed, and all turning maneuvers are completely coordinated. The equations of motion are written using the inertial coordinate system illustrated in Figure 2. The origin of the coordinate system is at the runway touchdown point; the x-axis is in the horizontal plane, parallel to the runway and positive in the landing direction; the z-axis is positive down along the local vertical; and the y-axis forms a right-hand orthogonal system. It should be noted that the flight path angle γ is positive below the local horizontal and the bank angle ϕ denotes a rotation of the lift vector about the velocity vector and away from the vertical plane.

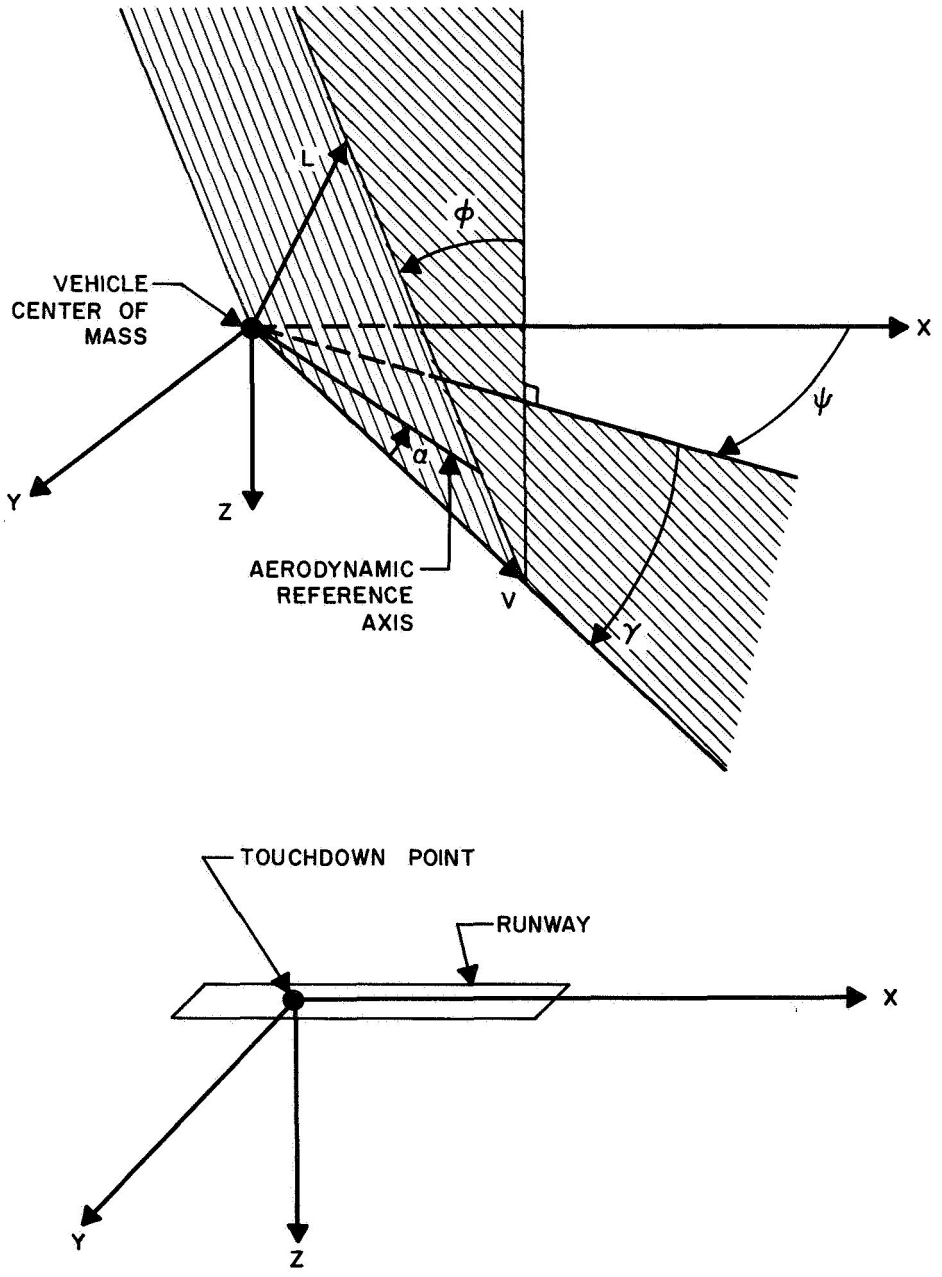

FIGURE 2. DEFINITION OF COORDINATE SYSTEM AND IMPORTANT PARAMETERS

$$m\dot{V} = -D + mg \sin\gamma \quad (1)$$

$$mV\dot{\gamma} = -L\cos\phi + mg\cos\gamma \quad (2)$$

$$mV\cos\gamma\,\dot{\psi} = L\sin\phi \quad (3)$$

$$\dot{x} = V\cos\gamma\cos\psi \quad (4)$$

$$\dot{y} = V\cos\gamma\sin\psi \quad (5)$$

$$\dot{z} = V\sin\gamma \quad (6)$$

The notation employed in Equations (1)-(6) is standard and the symbols are defined in the Glossary of Symbols at the beginning of this report.

The six state variables of the system are the velocity V, the flight path angle γ, the heading angle ψ, and the position coordinates x, y, and z; the angle of attack α and the bank angle ϕ are the control variables. In the following subsection, the number of state variables will be reduced by the introduction of suitable approximations.

2.2 SIMPLIFIED EQUATIONS

2.2.1 Quasi-Steady Approximation

The vehicles considered in Reference 6 were found to approach a quasi-equilibrium glide at constant α and ϕ for a wide range of initial conditions. That is, $\dot{V}$ and $\dot{\gamma}$ become so small that the values of V and γ are essentially determined by the equilibrium conditions at the local altitude. Hence, for a given α and ϕ, V and γ are only functions of altitude. For example, Figure 3 shows that both velocity and flight path angle for a 360^{o} approach become quasi-steady below an altitude of about 9 km.

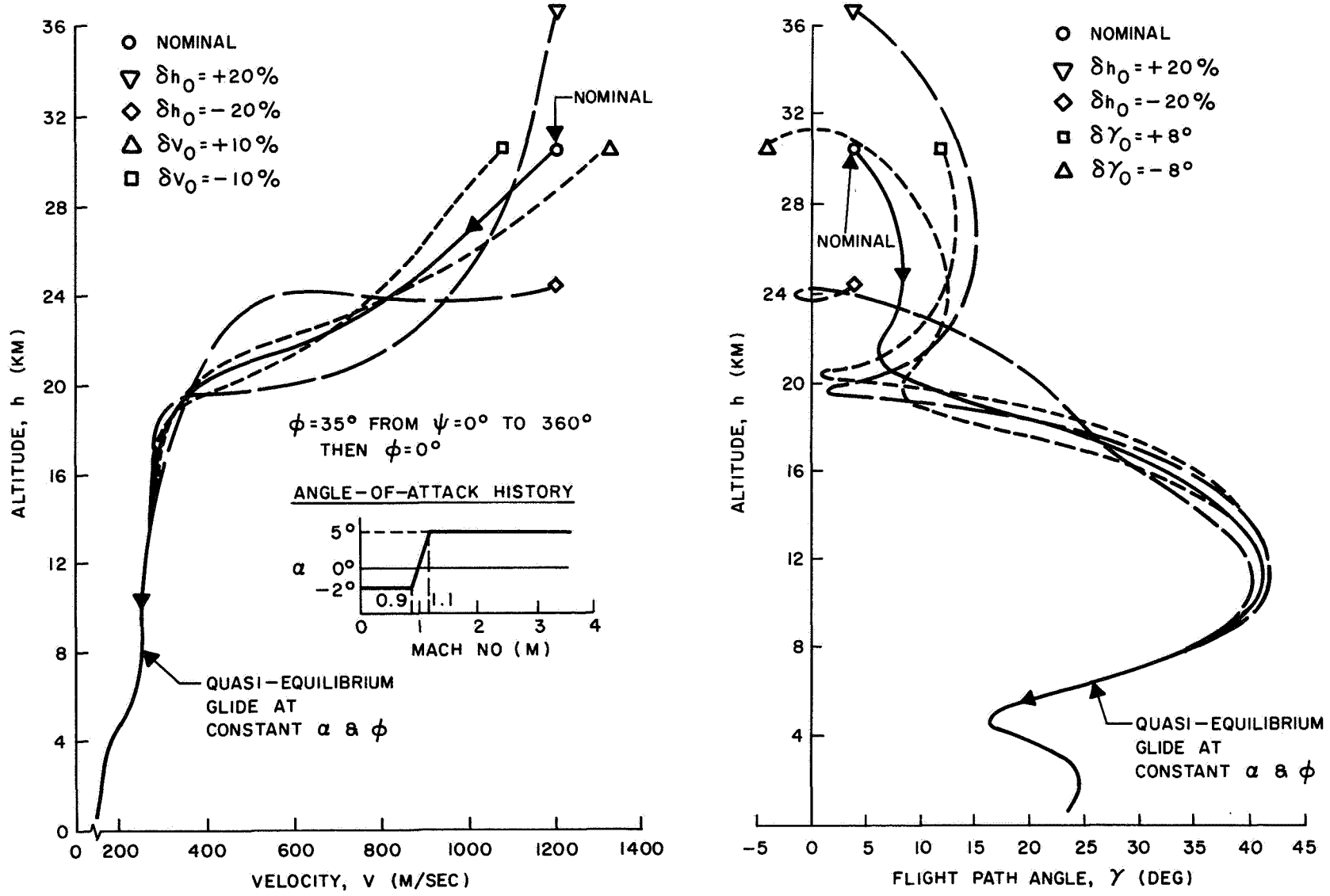

(a) Velocity vs Altitude

(b) Flight Path Angle vs Altitude

FIGURE 3. QUASI-EQUILIBRIUM GLIDE

By assuming that V and γ change slowly along the flight path, we may neglect $\dot{V}$ and $\dot{\gamma}$ in the equations of motion. With these approximations, Equations (1) through (3) simplify to

$$D = mg \sin\gamma \tag{7}$$

$$L = mg \cos\gamma \sec\phi \tag{8}$$

$$\dot{\psi} = \frac{g \tan\phi}{V} \tag{9}$$

The flight path is approximated by a descending helix with slowly changing helix angle γ and radius R given by (see Figure 4):

$$R = \frac{V \cos\gamma}{\dot{\psi}} = \frac{V^2 \cos\gamma}{g \tan\phi} \tag{10}$$

Equations (7) and (8) implicitly determine the quasi-steady flight path angle and velocity as functions of α and ϕ.

The quasi-steady approximation reduces the number of state variables to four by eliminating velocity and flight path angle. If the vertical position coordinate z is used

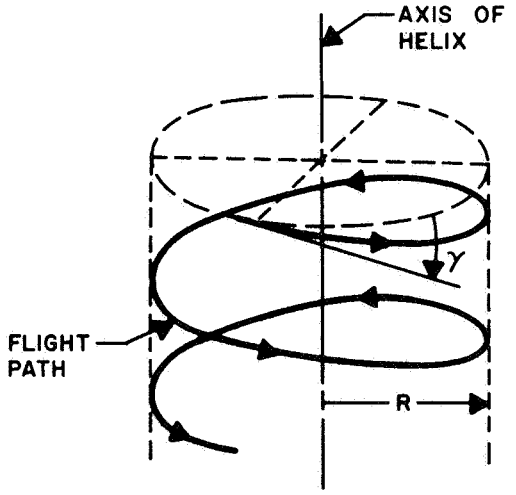

FIGURE 4. FLIGHT PATH AS A LOCALLY DESCENDING HELIX

instead of time as the independent variable, the motion of the glider may be expressed in terms of only three state variables. By dividing Equation (6) into Equations (4), (5) and (9), and then using Equation (10), we obtain the following simplified equations:

$$\frac{dx}{dz} = \text{ctn}\,\gamma\,\cos\psi \tag{11}$$

$$\frac{dy}{dz} = \text{ctn}\,\gamma\,\sin\psi \tag{12}$$

$$\frac{d\psi}{dz} = \frac{1}{R}\,\text{ctn}\,\gamma \tag{13}$$

The state variables of the system are now, x, y and ψ; the independent variable is z; and the control variables may be considered to be either γ and R or α and ϕ. The more common variables α and ϕ are related to γ and R through Equations (7), (8) and (10). However, to explicitly establish this relationship, the aerodynamic lift and drag characteristics of the glider must be specified. These are discussed next.

2.2.2 Aerodynamic Approximation

The point-mass aerodynamics of lifting entry vehicles may be closely approximated by assuming lift to be linear and drag to be quadratic in angle of attack, i.e.,

$$L = \frac{1}{2}\rho V^2 S_{ref} C_{L_\alpha}(\alpha - \alpha_o) \tag{14}$$

$$D = \frac{1}{2}\rho V^2 S_{ref} [C_{D_o} + \eta\, C_{L_\alpha}(\alpha - \alpha_o)^2] \tag{15}$$

where

ρ = local atmospheric density

S_{ref} = aerodynamic reference area

C_{L_α} = lift coefficient slope

α_o = angle of attack for zero lift

C_{D_o} = zero-lift drag coefficient

η = efficiency factor ($0 \leq \eta \leq 1$)

In general, C_{L_α}, α_o, C_{D_o} and η are functions of Mach number. However, for subsonic flight these quantities are very nearly constant.

As shown in Appendix E of Reference 7, the approximations of Equations (14) and (15) may be used to rewrite Equations (7), (8) and (10) as:

$$\frac{V^2}{g\ell} = \frac{\cos\gamma}{\bar{\alpha}\cos\phi} \tag{16}$$

$$\tan\gamma = \left(\bar{\alpha} + \frac{\delta^2}{4\bar{\alpha}}\right)\sec\phi \tag{17}$$

$$R = \frac{\ell\cos^2\gamma}{\bar{\alpha}\sin\phi} \tag{18}$$

where

$$\ell = \frac{2m\eta}{\rho C_{L_\alpha} S_{ref}} = \text{characteristic length}$$

$$\delta = 2\sqrt{\frac{\eta C_{D_o}}{C_{L_\alpha}}} = \text{minimum drag/lift ratio}$$

$$\bar{\alpha} = \eta(\alpha - \alpha_o) = \text{modified angle of attack}$$

The characteristic length ℓ is the only parameter in these equations which is a function of altitude (through the atmospheric density ρ).

Equations (16) and (17) explicitly determine the quasi-steady velocity and flight path angle in terms of the altitude and the control variables $\bar{\alpha}$ and ϕ. On the other hand, Equations (17) and (18) provide an implicit relationship between the control variables $(\bar{\alpha},\phi)$ and those appearing in the simplified equations of motion (γ,R). Figure 5 displays this latter relationship for the M-2 configuration during subsonic flight. The ratio ℓ/R has been plotted on the ordinate rather than R itself for two reasons: (1) R becomes infinite when $\phi = 0$, and (2) this removes the altitude dependence of the relationship. There are actually two values of $\bar{\alpha}$ and ϕ which satisfy Equations (17) and (18) for each γ and ℓ/R; only the solutions for the lower value of $\bar{\alpha}$ is shown in the figure since this corresponds to the region which pilots prefer.

The simplified system is specified by Equations (11)-(13), (17) and (18). At any altitude, the selected values of the control variables α and ϕ may be used to determine R and γ by means of a chart like Figure 5. These, together with the current values of the state variables (x,y,ψ), completely determine the rates of change of (x,y,ψ) with altitude.

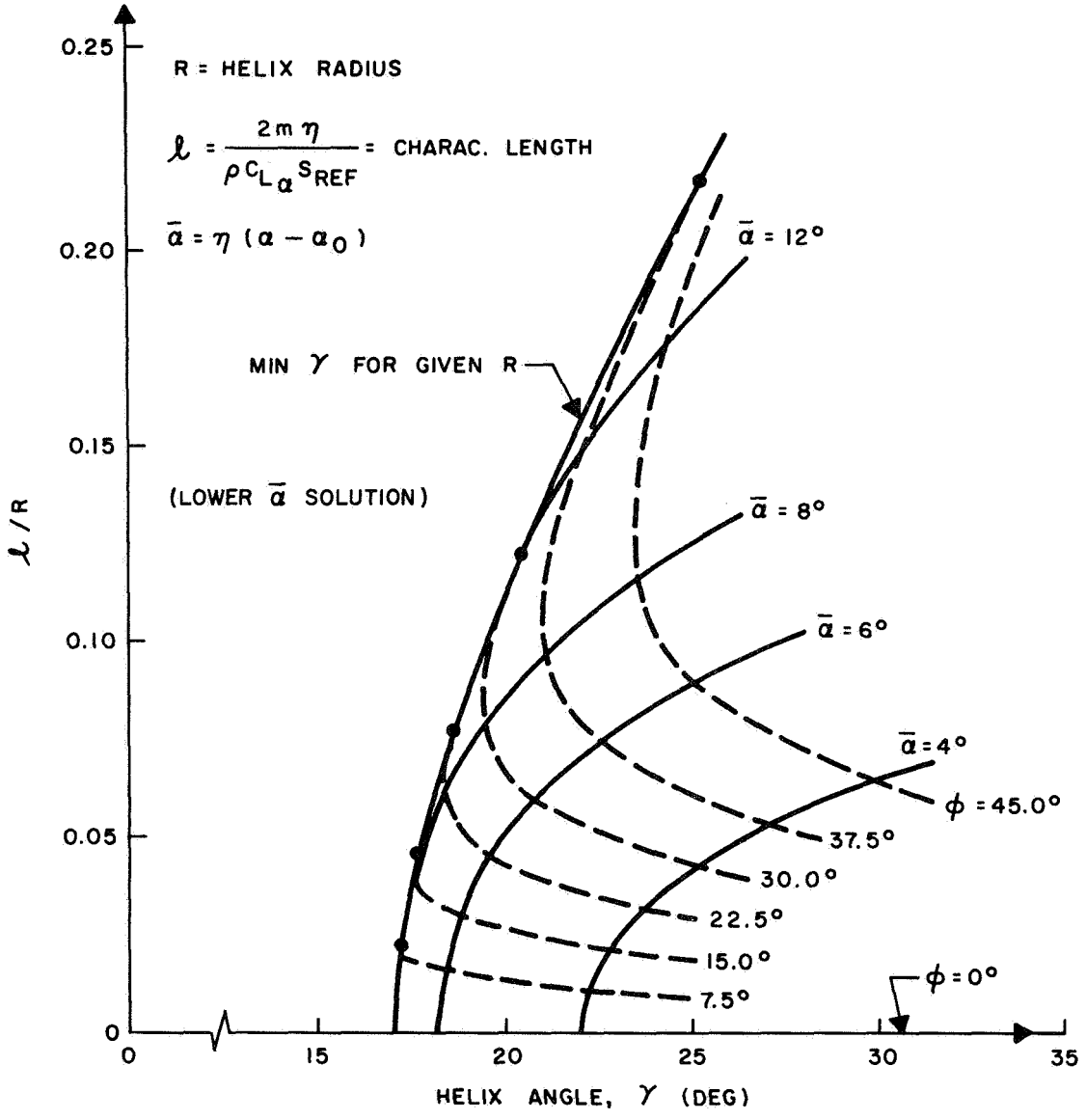

FIGURE 5. HELIX RADIUS VS HELIX ANGLE FOR VARIOUS VALUES OF BANK ANGLE AND MODIFIED ANGLE OF ATTACK

2.3 PERTURBATION EQUATIONS

The simplified equations of motion are still nonlinear and the physical control variables α and ϕ enter into them implicitly. The application of the synthesis technique to be described later requires the equations of motion to be linear in both the state and control variables. This may be accomplished by taking first-order perturbations of the equations of motion about a nominal trajectory.

Using vector-matrix notation, the perturbation form of Equations (11) - (13) may be written as

$$\frac{d}{dz}\begin{bmatrix}\delta x\\ \delta y\\ \delta\psi\end{bmatrix} = \begin{bmatrix}0, & 0, & -\text{ctn}\,\gamma\sin\psi\\ 0, & 0, & \text{ctn}\,\gamma\cos\psi\\ 0, & 0, & 0\end{bmatrix}_N\begin{bmatrix}\delta x\\ \delta y\\ \delta\psi\end{bmatrix} + \begin{bmatrix}-\cos\psi\csc^2\gamma, & 0\\ -\sin\psi\csc^2\gamma, & 0\\ -\frac{1}{R}\csc^2\gamma, & -\frac{1}{R^2}\text{ctn}\,\gamma\end{bmatrix}_N\begin{bmatrix}\delta\gamma\\ \delta R\end{bmatrix} \tag{19}$$

where the subscript N indicates the quantity is evaluated along the nominal trajectory, and

$$\delta\psi = \psi-\psi_N, \quad \delta x = x-x_N, \quad \delta y = y-y_N,$$
$$\delta\gamma = \gamma-\gamma_N, \quad \delta R = R-R_N$$

Similarly, the perturbation versions of Equations (17) and (18) are

$$\begin{bmatrix}\delta\gamma\\ \delta R\end{bmatrix} = \begin{bmatrix}\frac{\partial\gamma}{\partial\alpha}, & \frac{\partial\gamma}{\partial\phi}\\ \frac{\partial R}{\partial\alpha}, & \frac{\partial R}{\partial\phi}\end{bmatrix}_N\begin{bmatrix}\delta\alpha\\ \delta\phi\end{bmatrix} \tag{20}$$

where the elements of the matrix are

$$\frac{\partial\gamma}{\partial\alpha} = \eta\left(1 - \frac{\delta^2}{4\bar{\alpha}^2}\right)\cos^2\gamma \sec\phi \tag{21}$$

$$\frac{\partial\gamma}{\partial\phi} = \frac{\sin 2\gamma \tan\phi}{2} \tag{22}$$

$$\frac{\partial R}{\partial\alpha} = -\eta R\left[\frac{1}{\bar{\alpha}} + \frac{\sin 2\gamma}{\cos\phi}\left(1 - \frac{\delta^2}{4\bar{\alpha}^2}\right)\right] \tag{23}$$

$$\frac{\partial R}{\partial\phi} = -R\left[\operatorname{ctn}\phi + 2\tan\phi \sin^2\gamma\right] \tag{24}$$

and

$$\delta\alpha = \alpha - \alpha_N, \qquad \delta\phi = \phi - \phi_N$$

The substitution of Equation (20) into Equation (19) leads to the desired set of linear perturbation equations:

$$\frac{d\bar{x}}{dz} = F\bar{x} + G\bar{u} \tag{25}$$

where the state vector $\bar{x}$ and the control vector $\bar{u}$ are defined as

$$\bar{x} = \begin{bmatrix} \delta x \\ \delta y \\ \delta\psi \end{bmatrix} \tag{26}$$

$$\bar{u} = \begin{bmatrix} \delta\alpha \\ \delta\phi \end{bmatrix} \tag{27}$$

and the matrices F and G are given by

$$F = \begin{bmatrix} 0 & 0 & -\operatorname{ctn}\gamma \sin\psi \\ 0 & 0 & \operatorname{ctn}\gamma \cos\psi \\ 0 & 0 & 0 \end{bmatrix}_N \tag{28}$$

$$G = \begin{bmatrix} -\cos\psi \csc^2\gamma, & 0 \\ -\sin\psi \csc^2\gamma, & 0 \\ -\frac{1}{R}\csc^2\gamma, & -\frac{1}{R^2}\operatorname{ctn}\gamma \end{bmatrix}_N \begin{bmatrix} \frac{\partial\gamma}{\partial\alpha}, & \frac{\partial\gamma}{\partial\phi} \\ \frac{\partial R}{\partial\alpha}, & \frac{\partial R}{\partial\phi} \end{bmatrix}_N \qquad (29)$$

2.4 TERMINAL GUIDANCE FOR QUADRATIC PERFORMANCE CRITERIA

Having described the approximate motion of the vehicle in the vicinity of the nominal trajectory, we now wish to find a feedback law for the control variables $\delta\alpha$ and $\delta\phi$ which will guide the glider from a condition off the nominal trajectory to the desired terminal conditions while exhibiting acceptable behavior along the way. A convenient performance index to choose (Reference 15), the minimization of which leads to linear feedback control, is one which is quadratic in both the state and the control variables. The general form is

$$J = \frac{1}{2}\left(\bar{x}^T S_f \bar{x}\right)_{z=z_f} + \frac{1}{2}\int_{z_o}^{z_f}\left(\bar{x}^T A\bar{x} + \bar{u}^T B\bar{u}\right)dz \qquad (30)$$

where z_o and z_f are, respectively, the initial and final values of the independent variable. The weighting matrices S_f, A and B are to be chosen by the designer. The matrix S_f, which must be positive semi-definite, penalizes the terminal errors in the state variables, while matrix A penalizes the en route deviations of the state variables from nominal. The use of control deviations is penalized by matrix B, which must be positive definite.

A reasonable choice of these matrices for the entry vehicle guidance scheme is

$$S_f = \begin{bmatrix} \frac{1}{\delta x_f^2} & 0 & 0 \\ 0 & \frac{1}{\delta y_f^2} & 0 \\ 0 & 0 & \frac{1}{\delta \psi_f^2} \end{bmatrix} \tag{31}$$

$$A = 0 \tag{32}$$

$$B = \begin{bmatrix} \frac{1}{\delta \alpha_o^2} & 0 \\ 0 & \frac{1}{\delta \phi_o^2} \end{bmatrix} \tag{33}$$

Equations (31) and (32) imply that state variable errors (δx, δy, $\delta \psi$) are considered unimportant except at the final altitude. The parameters δx_f, δy_f, $\delta \psi_f$, $\delta \alpha_o$ and $\delta \phi_o$ must be chosen to provide satisfactory terminal accuracy within limitations of acceptable $\delta \alpha$ and $\delta \phi$. Usually, good estimates are the maximum allowable values.

The minimization of the performance criteria, Equation (30), subject to the perturbation equations of motion, Equation (25), yields the optimum feedback guidance law

$$\bar{u} = -C(z)\bar{x} \tag{34}$$

The feedback gain matrix C(z) is defined by

$$C = B^{-1} G^T S \tag{35}$$

where B^{-1} is the inverse of B, G^T is the transpose of G, and S is the solution of the matrix Riccati equation

$$\frac{dS}{dz} = -SF - F^T S + SGB^{-1} G^T S \tag{36}$$

with the boundary condition

$$S(z_f) = S_f \tag{37}$$

2.5 SUMMARY

The terminal guidance law is given by Equation (34), which may be rewritten in expanded form as

$$\begin{bmatrix} \alpha \\ \phi \end{bmatrix} = \begin{bmatrix} \alpha_N(h) \\ \phi_N(h) \end{bmatrix} - \begin{bmatrix} C_{\alpha x}(h), & C_{\alpha y}(h), & C_{\alpha \psi}(h) \\ C_{\phi x}(h), & C_{\phi y}(h), & C_{\phi \psi}(h) \end{bmatrix} \begin{bmatrix} x - x_N(h) \\ y - y_N(h) \\ \psi - \psi_N(h) \end{bmatrix} \tag{38}$$

The altitude h has been used instead of the position coordinate z for convenience, where

$$h = h_R - z \tag{39}$$

and h_R is the altitude of the runway above sea level.

The terminal guidance scheme is summarized in Figures 6 and 7. Figure 6 is a block diagram showing how the system would be implemented onboard a lifting body vehicle. A nominal trajectory would be selected and used to pre-calculate the feedback gains. Next, the nominal state histories $[x_N(h), y_N(h), \psi_N(h)]$, the nominal control histories

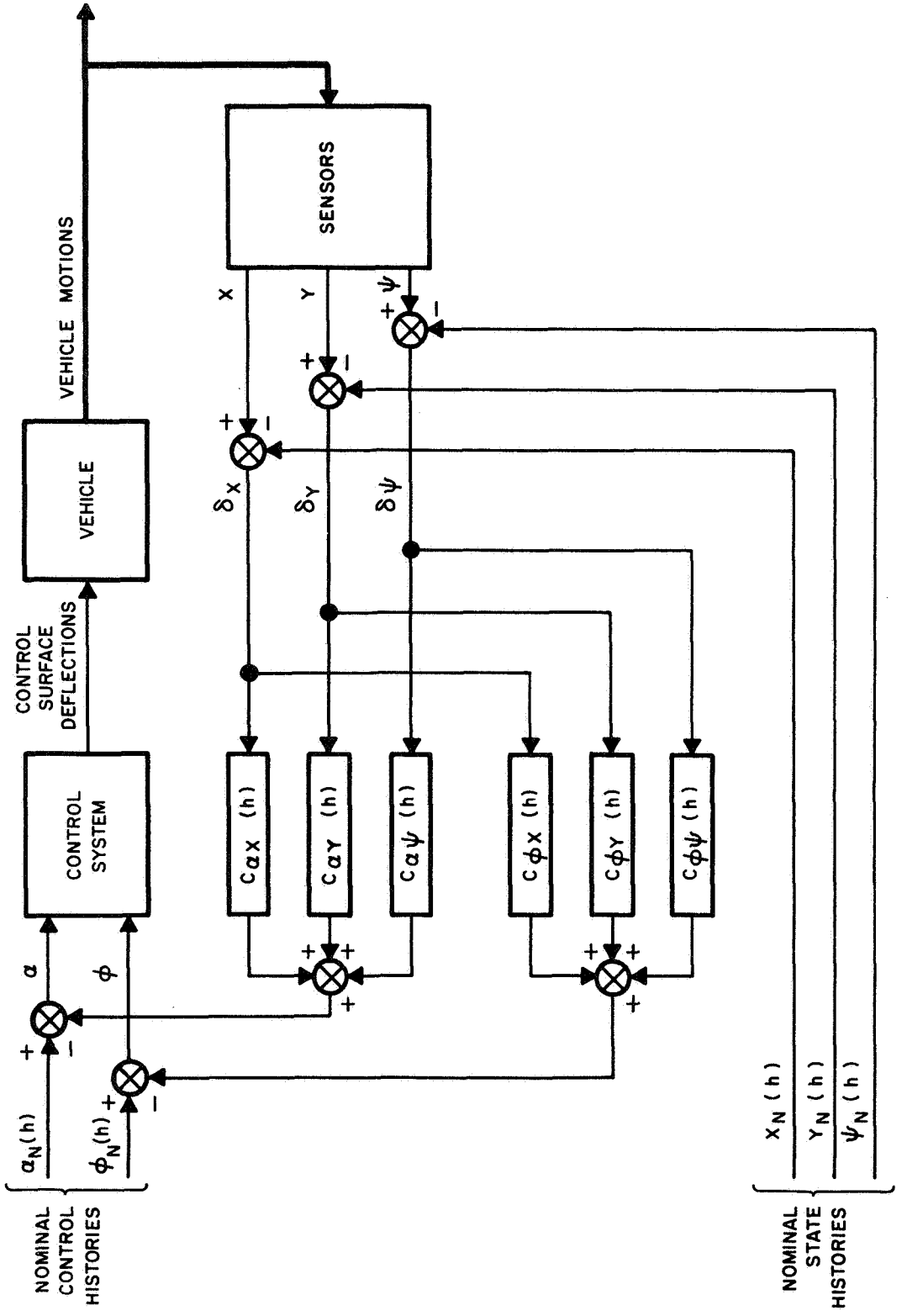

FIGURE 6. BLOCK DIAGRAM OF TERMINAL GUIDANCE SCHEME

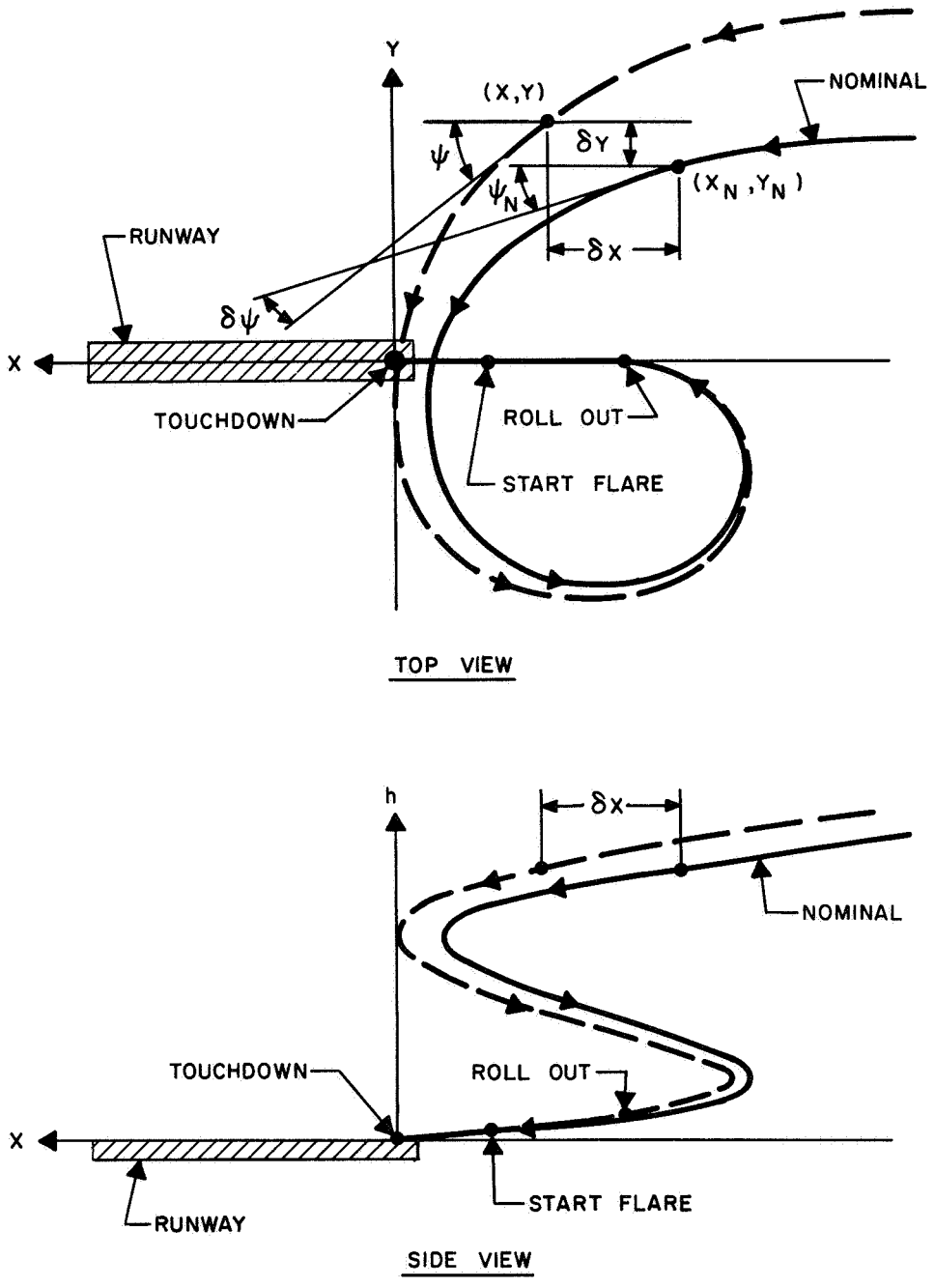

FIGURE 7. TYPICAL PERFORMANCE OF TERMINAL GUIDANCE SCHEME

$[\alpha_N(h), \phi_N(h)]$, and the feedback gains $[C_{\alpha x}(h), C_{\alpha y}(h), C_{\alpha \psi}(h), C_{\phi x}(h), C_{\phi y}(h), C_{\phi \psi}(h)]$ would be stored as functions of altitude in the airborne computer. During the terminal phase of the flight, the actual state variables (and the altitude) would be measured and compared with the nominal values for that altitude. The errors would then be used to properly modify the stored nominal control histories by means of Equation (38).

The operation of the scheme is illustrated in Figure 7, which shows horizontal and vertical projections of the nominal trajectory (solid) and a typical off-nominal one (dashed) for a 360^o approach. The actual and nominal values of the state variables, and the deviations themselves, are indicated for a particular altitude. Notice that the terminal guidance scheme does not attempt to restore the vehicle to the nominal path, but instead it smoothly "funnels" the vehicle from its off-nominal condition down to the desired terminal conditions.

SECTION III

SYSTEM PERFORMANCE

The performance of the terminal guidance scheme developed in the previous section was evaluated by means of a digital computer simulation, which used the full six state variable model of Equations (1)-(6) and the aerodynamic/mass characteristics of the NASA M-2 lifting body. Details of the simulation program and the vehicle characteristics may be found in Reference 6. The following subsections describe the selection of the nominal trajectories, the calculation of the corresponding feedback gains, and the performance of the system for a variety of off-nominal conditions.

3.1 NOMINAL TRAJECTORIES

Two nominal trajectories were selected for the numerical evaluation of the terminal guidance scheme: (1) a straight-in approach, and (2) a 90^{o} approach. Both of these consist of a glide from an initial altitude of 9.0 km to a final (start-flare) altitude of 1.2 km at a constant flight path angle of 21^{o}. For the straight-in approach, the vehicle is assumed to be initially unbanked and flying in the vertical plane containing the runway centerline. In the 90^{o} approach, the glider is initially headed perpendicular to the runway and is banked at an angle of -30^{o}. This bank angle is held until a 90^{o} heading change has been executed and the glider is lined up with the runway. At this point, a roll-out maneuver is performed

(i.e., the bank angle is switched to 0^{o}) and the vehicle proceeds along a straight-in approach to the final altitude. These two nominals are not particularly recommended for actual use, but were merely selected as representative maneuvering and non-maneuvering approaches.

As stated in the Introduction, this investigation was limited to the subsonic flight regime in order to render the aerodynamic coefficients constant with Mach number. In particular, the nominal initial velocity for both approaches was selected as 240 m/sec, which corresponds to a Mach number of 0.79 at the initial altitude. The initial downrange and crossrange coordinates are such that, at the start-flare altitude, the glider is located on the runway axis 3.5 km short of touchdown. The flare maneuver was assumed to commence at an altitude of 1.2 km (500 m above the runway which is situated 700 m above sea level). Table I summarizes the initial conditions for both nominal approaches.

TABLE I. NOMINAL INITIAL CONDITIONS

Initial Condition / Approach	h_o (m)	V_o (m/sec)	γ_o (deg)	ψ_o (deg)	ϕ_o (deg)	x_o (m)	y_o (m)
Straight-In	9000	240	21	0	0	-23820	0
90-Degree	9000	240	21	90	-30	-19006	-8025

The two nominal approaches are illustrated in Figures 8 and 9. The first figure shows the projections of the trajectories onto the horizontal and vertical planes containing the runway (these are the ground track, and the altitude versus downrange plot, respectively). The second figure presents the flight path angle, the velocity, and the nominal control histories (angle of attack and bank angle) as functions of altitude.

3.2 FEEDBACK GAINS

The nominal trajectory data of Figure 9 were used to calculate a set of feedback gains for each of the two approaches. Table II summarizes the subsonic aerodynamic parameters assumed for the example. The variation of the characteristic length ℓ with altitude is shown in Figure 10. The weighting functions which specify the matrices S_f and B in Equations (31) and (33) were chosen to represent reasonable allowable values for the respective quantities. These are also summarized in Table II.

The feedback gains are shown in Figures 11 and 12. In general, their magnitudes are small at the initial altitude (9000 m) and grow larger as the glider descends. For the 90^o approach, a discontinuity occurs in each of the gains at the roll-out altitude (4470 m) where the nominal bank angle switches from -30^o to 0^o. Below this altitude, the gains for the two approaches are practically identical since the vehicle is gliding straight in both cases. During the straight-in glide, the gains $C_{\alpha y}$, C_{α_ψ} and $C_{\phi x}$ are all zero; in other words, the longitudinal

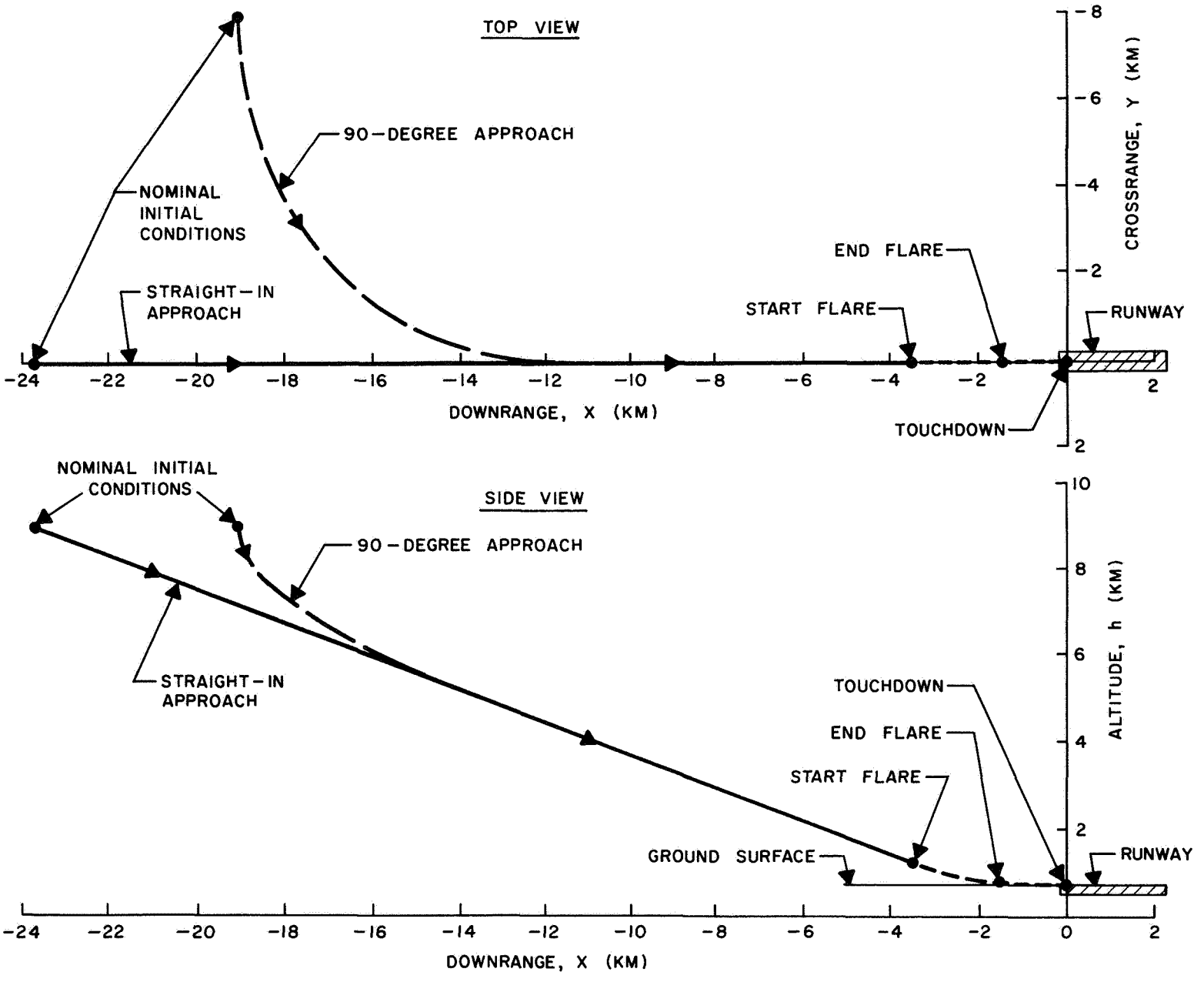

FIGURE 8. NOMINAL TRAJECTORY PROFILES

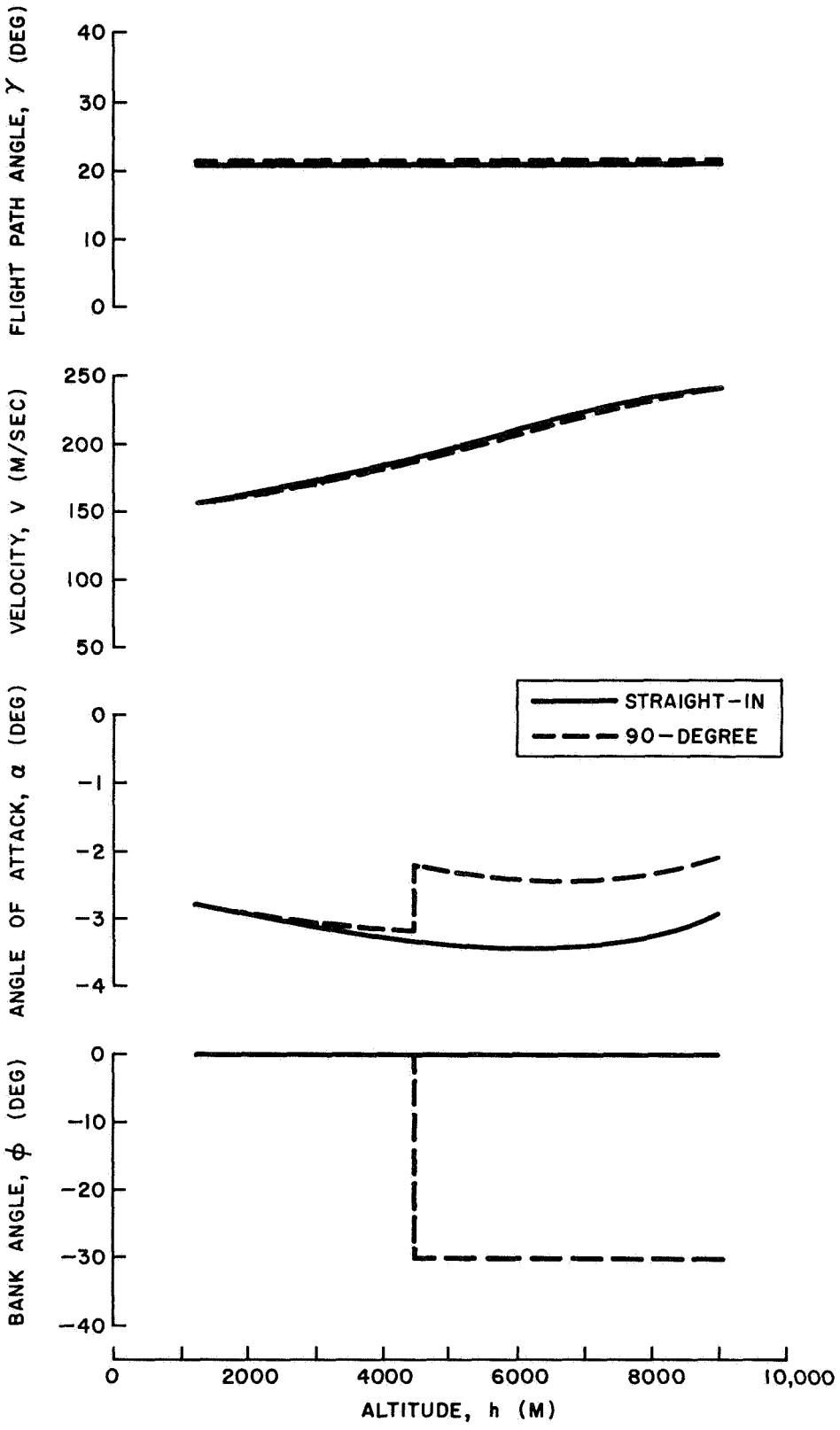

FIGURE 9. NOMINAL TRAJECTORY HISTORIES

TABLE II. VALUES USED TO CALCULATE FEEDBACK GAINS

	Item	Units	Value
Aerodynamic Parameters	C_{L_α}	deg^{-1}	0.0223
	α_o	deg	-9.48
	C_{D_o}	——	0.05946
	η	deg^{-1}	0.00702
	δ	——	0.2737
Weighting Functions	δx_f	m	100.0
	δy_f	m	50.0
	$\delta \psi_f$	deg	1.0
	$\delta \alpha_o$	deg	3.0
	$\delta \Phi_o$	deg	30.0

and lateral-directional modes are decoupled. Errors in cross-range position or heading angle do not influence the angle of attack, and downrange position errors do not affect the bank angle.

In the simulation, only the values of the gains for a few selected altitudes are stored and linear interpolation is

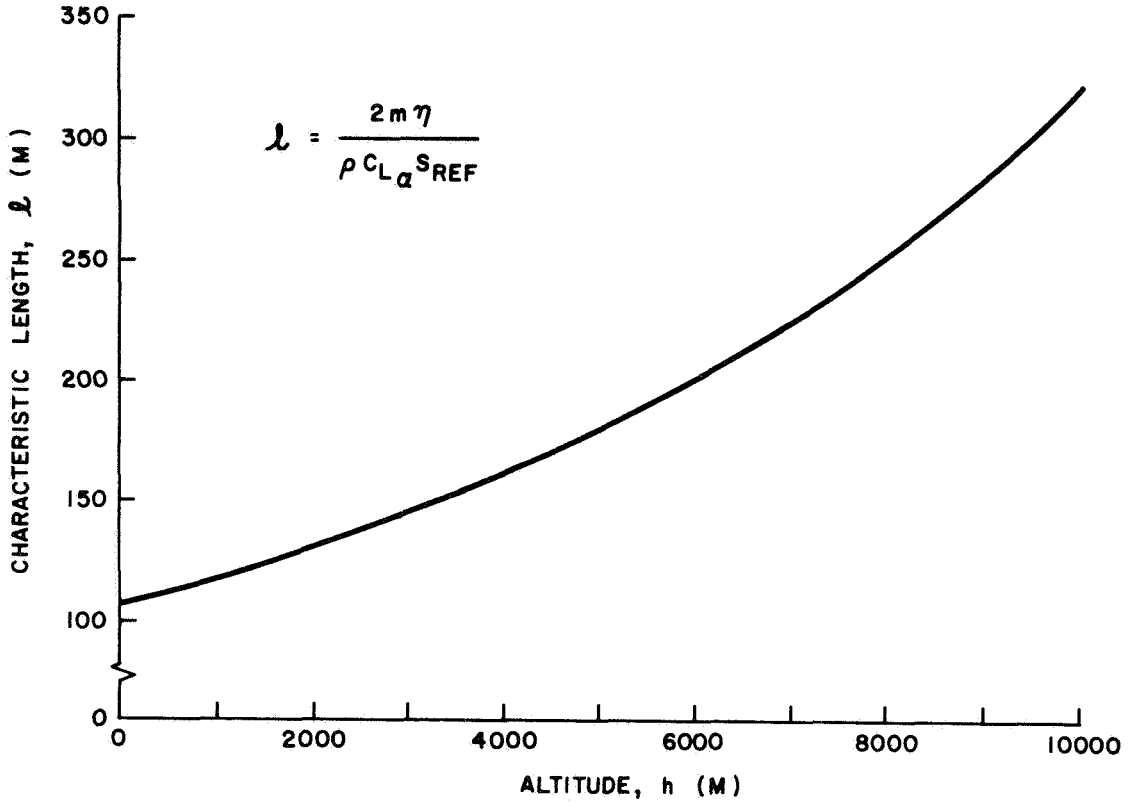

FIGURE 10. CHARACTERISTIC LENGTH VERSUS ALTITUDE

used to calculate the gains for intermediate altitudes. Initially, the altitudes selected were at 500 m intervals, beginning at the start-flare altitude. However, this resulted in unsatisfactory performance in the lowest altitude interval where the gains change rapidly and the linear approximation is very poor; relatively small state variable errors resulted in extremely large guidance commands. Consequently, this

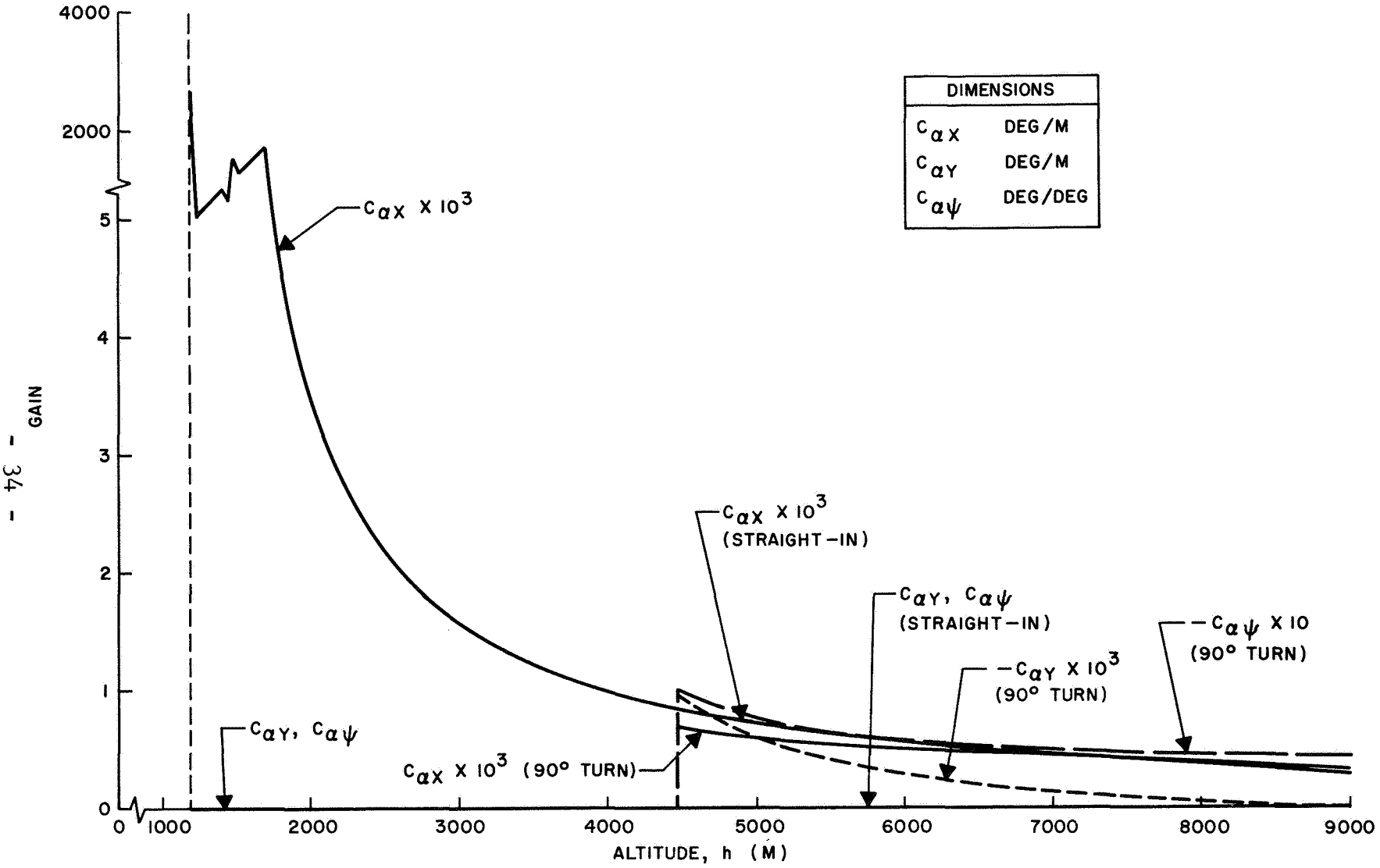

FIGURE 11. ANGLE OF ATTACK FEEDBACK GAINS VERSUS ALTITUDE

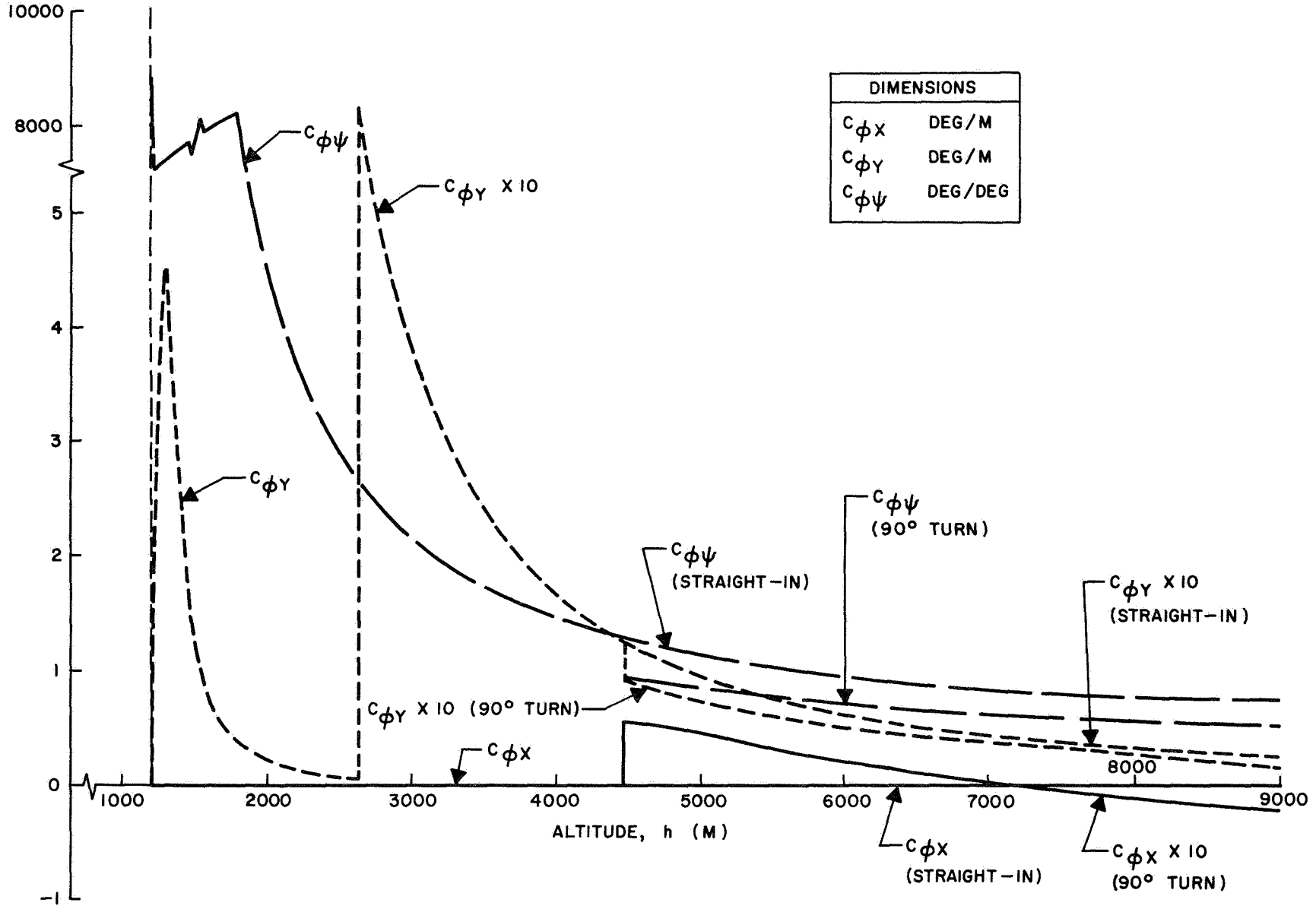

FIGURE 12. BANK ANGLE FEEDBACK GAINS VERSUS ALTITUDE

interval was subdivided into finer segments. The results were vastly improved, but in a few cases the control demands in the lowest interval were still exorbitant. To remedy this situation, the terminal values of the feedback gains $C_{\alpha x}$ and $C_{\phi\psi}$ were modified to provide a better linear approximation to the actual curves. Tables III and IV list the final values used in the simulation for the altitude intervals, the feedback gains and the nominal state and control variable histories.

3.3 INITIAL CONDITION ERRORS

The first off-nominal situations investigated were deviations in the initial conditions, i.e. conditions at h = 9 km. Both individual and combined errors were considered.

3.3.1 Individual Errors

Figures 13 and 14 show the performance for the straight-in approach with very large initial position and heading errors. Figure 13 is an altitude-downrange plot which shows the nominal trajectory and those resulting from initial downrange errors of ± 3000 m. The terminal guidance scheme very nicely "funnels" the glider from its off-nominal initial position right into the nominal start-flare point. The ground tracks for the nominal, for initial heading errors of ± 5000 m, and for initial crossrange errors of ± 50^{o} are shown in Figure 14. Again the guidance scheme is seen to perform very well.

TABLE III. GUIDANCE PARAMETERS FOR STRAIGHT - IN APPROACH

h (m)	X_N (m)	Y_N (m)	ψ_N (deg)	α_N (deg)	ϕ_N (deg)	$C_{\alpha x} \times 10^3$ (deg/m)	$C_{\alpha y}$ (deg/m)	$C_{\alpha \psi}$ (deg/deg)	$C_{\phi x}$ (deg/m)	$C_{\phi y} \times 10$ (deg/m)	$C_{\phi \psi}$ (deg/deg)
1200	- 3500	0	0	-2.81	0	31.51*	0	0	0	0.0	25.00*
1300	- 3761	0	0	-2.83	0	22.63	0	0	0	44.61	20.20*
1400	- 4021	0	0	-2.84	0	13.86	0	0	0	24.08	15.39
1500	- 4282	0	0	-2.86	0	9.25	0	0	0	12.17	11.30
1700	- 4803	0	0	-2.89	0	5.56	0	0	0	4.62	7.10
2200	- 6105	0	0	-2.98	0	2.78	0	0	0	1.19	3.69
2700	- 7408	0	0	-3.07	0	1.86	0	0	0	.54	2.54
3200	- 8711	0	0	-3.15	0	1.39	0	0	0	.31	1.96
3700	-10013	0	0	-3.23	0	1.11	0	0	0	.20	1.62
4200	-11316	0	0	-3.30	0	.92	0	0	0	.14	1.39
4700	-12618	0	0	-3.35	0	.78	0	0	0	.11	1.23
5200	-13921	0	0	-3.40	0	.68	0	0	0	.08	1.11
5700	-15223	0	0	-3.43	0	.60	0	0	0	.07	1.01
6200	-16526	0	0	-3.44	0	.53	0	0	0	.06	.94
6700	-17828	0	0	-3.42	0	.47	0	0	0	.05	.88
7200	-19131	0	0	-3.38	0	.42	0	0	0	.04	.83
7700	-20433	0	0	-3.30	0	.37	0	0	0	.04	.79
8200	-21736	0	0	-3.19	0	.33	0	0	0	.03	.75
8700	-23038	0	0	-3.04	0	.30	0	0	0	.03	.73
9000	-23820	0	0	-2.92	0	.28	0	0	0	.03	.71

*Modified values

TABLE IV. GUIDANCE PARAMETERS FOR 90° APPROACH

h (m)	X_N (m)	Y_N (m)	ψ_N (deg)	α_N (deg)	ϕ_N (deg)	$C_{\alpha x} \times 10^3$ (deg/m)	$C_{\alpha y} \times 10^3$ (deg/m)	$C_{\alpha\psi} \times 10^2$ (deg/deg)	$C_{\phi x} \times 10$ (deg/m)	$C_{\phi y} \times 10$ (deg/m)	$C_{\phi\psi}$ (deg/deg)
1200	- 3500	0	0	-2.79	0	31.51*	0.0	0.0	0.0	0.0	25.00*
1300	- 3761	0	0	-2.80	0	22.63	0.0	0.0	0.0	44.65	20.20*
1400	- 4021	0	0	-2.82	0	13.96	0.0	0.0	0.0	24.02	15.35
1500	- 4282	0	0	-2.83	0	9.32	0.0	0.0	0.0	12.13	11.26
1700	- 4803	0	0	-2.86	0	5.60	0.0	0.0	0.0	4.60	7.07
2200	- 6105	0	0	-2.93	0	2.80	0.0	0.0	0.0	1.19	3.68
2700	- 7408	0	0	-3.01	0	1.87	0.0	0.0	0.0	.54	2.53
3200	- 8710	0	0	-3.07	0	1.40	0.0	0.0	0.0	.31	1.95
3700	-10013	0	0	-3.13	0	1.11	0.0	0.0	0.0	.20	1.61
4200	-11315	0	0	-3.17	0	.92	0.0	0.0	0.0	.14	1.38
4470	-12019	0	0	-3.19	0	.84	0.0	0.0	0.0	.12	1.28
4470	-12019	0	0	-2.20	-30	.70	- .95	-9.90	.05	.09	.97
4700	-12617	- 31	5.82	-2.24	-30	.64	- .75	-8.64	.05	.08	.93
5200	-13889	- 300	17.92	-2.32	-30	.56	- .49	-6.87	.04	.07	.84
5700	-15080	- 822	29.27	-2.38	-30	.51	- .33	-5.88	.03	.06	.75
6200	-16150	-1562	39.94	-2.42	-30	.48	- .23	-5.29	.02	.05	.68
6700	-17070	-2482	49.99	-2.44	-30	.45	- .16	-4.91	.01	.04	.63
7200	-17820	-3546	59.48	-2.42	-30	.42	- .10	-4.68	- .00	.03	.59
7700	-18390	-4715	68.49	-2.38	-30	.39	- .06	-4.52	- .01	.03	.57
8200	-18774	-5959	77.05	-2.30	-30	.36	- .02	-4.40	- .01	.02	.56
8700	-18973	-7245	85.24	-2.18	-30	.33	.00	-4.29	- .02	.02	.56
9000	-19006	-8025	90.00	-2.08	-30	.31	.01	-4.23	- .02	.02	.56

*Modified values

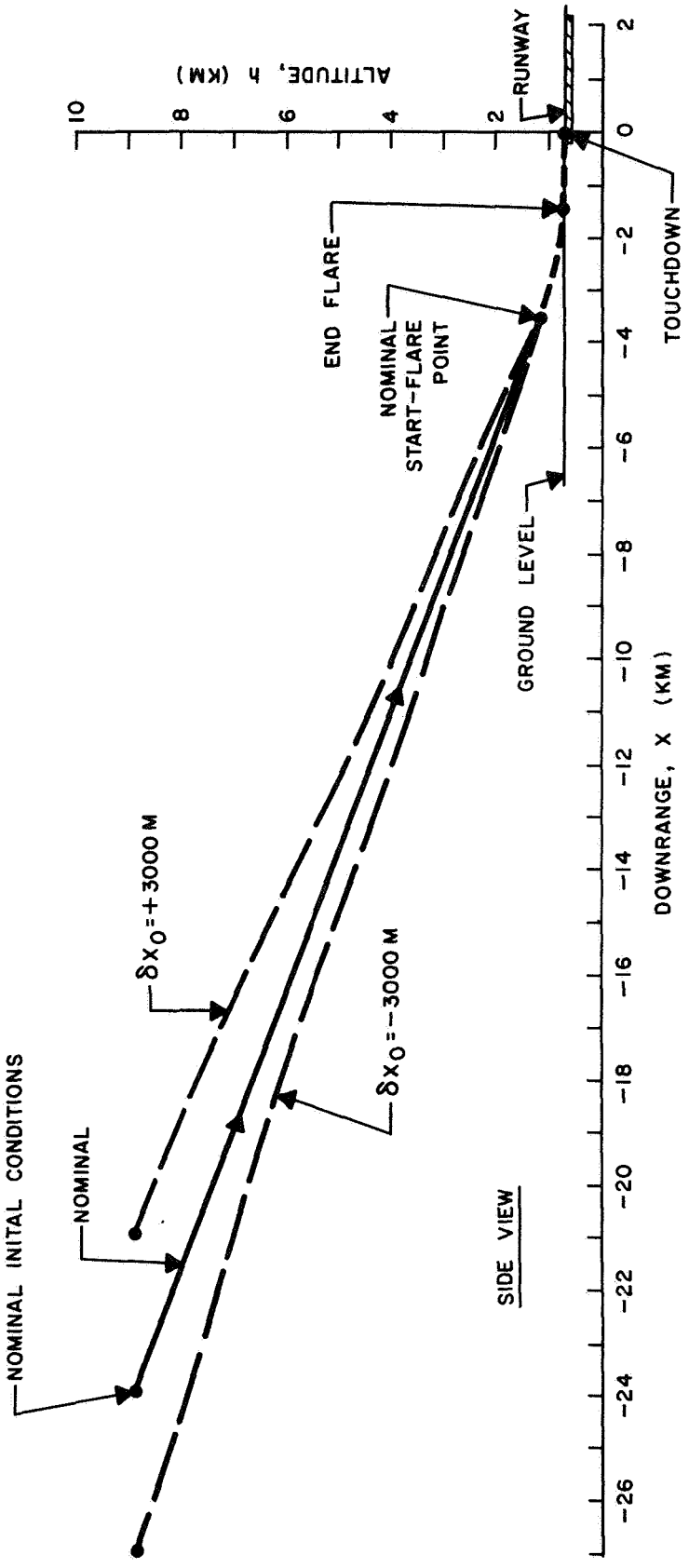

FIGURE 13. STRAIGHT-IN APPROACH WITH INITIAL DOWNRANGE ERRORS

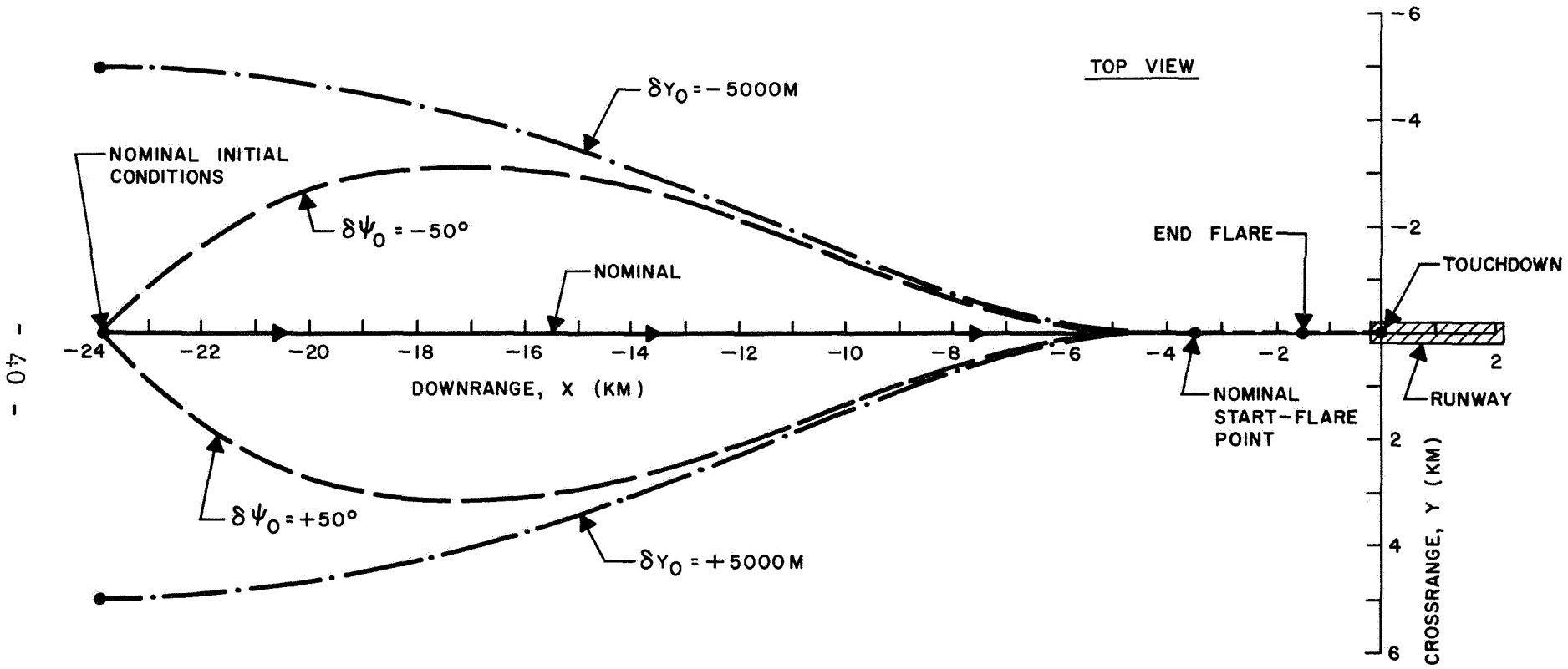

FIGURE 14. STRAIGHT-IN APPROACH WITH INITIAL CROSSRANGE AND HEADING ERRORS

The effects of the same initial condition errors for the 90^{o} approach are presented in Figures 15 and 16. It is apparent that the guidance scheme is very effective for the maneuvering approach as well.

The terminal errors themselves are not visible on the scales to which Figures 13 to 16 are plotted. Tables V and VI are included to clearly reveal the terminal accuracy of the guidance scheme for both approaches. These tables present

TABLE V. EFFECTS OF INDIVIDUAL INITIAL CONDITION ERRORS FOR STRAIGHT-IN APPROACH

Initial Condition Error	δx_f (m)	δy_f (m)	$\delta \psi_f$ (deg)	$\delta \gamma_f$ (deg)	δV_f (m/sec)
δx_o = + 3000 m	5.52	0.00	0.00	4.60	15.03
δx_o = - 3000 m	-16.47	0.00	0.00	-3.04	-14.14
δy_o = ± 5000 m	-14.03	∓0.03	∓0.03	-2.47	- 8.21
$\delta \psi_o$ = ± 50 deg	-22.18	∓0.00	∓0.01	-2.53	-15.94
$\delta \gamma_o$ = + 6 deg	13.09	0.00	0.00	0.63	- 2.82
$\delta \gamma_o$ = - 6 deg	-22.97	0.00	0.00	-0.08	2.93
δV_o = + 30 m/sec	1.94	0.00	0.00	1.93	4.21
δV_o = - 30 m/sec	21.55	0.00	0.00	-0.62	-8.10

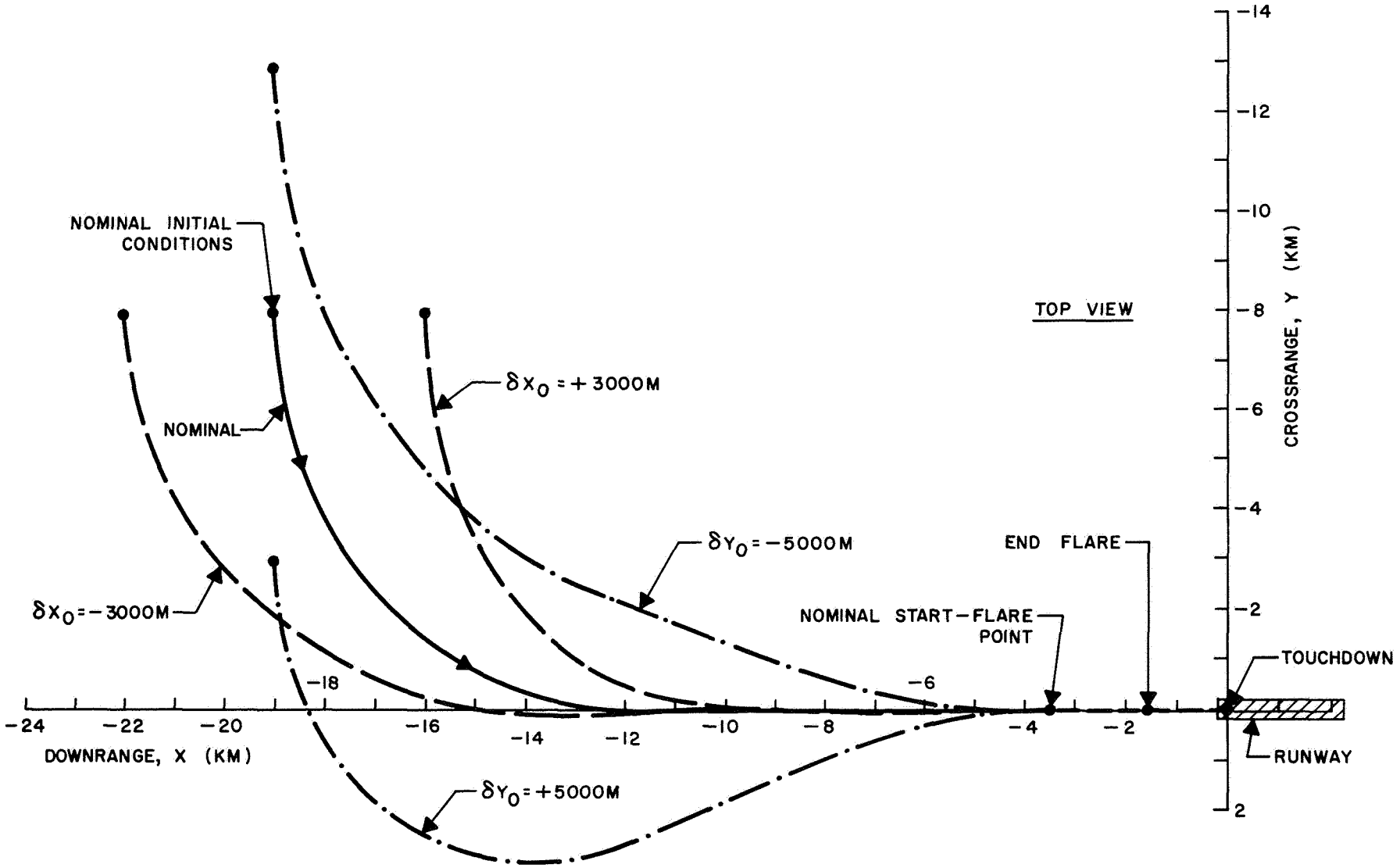

FIGURE 15. 90-DEGREE APPROACH WITH INITIAL DOWNRANGE AND CROSSRANGE ERRORS

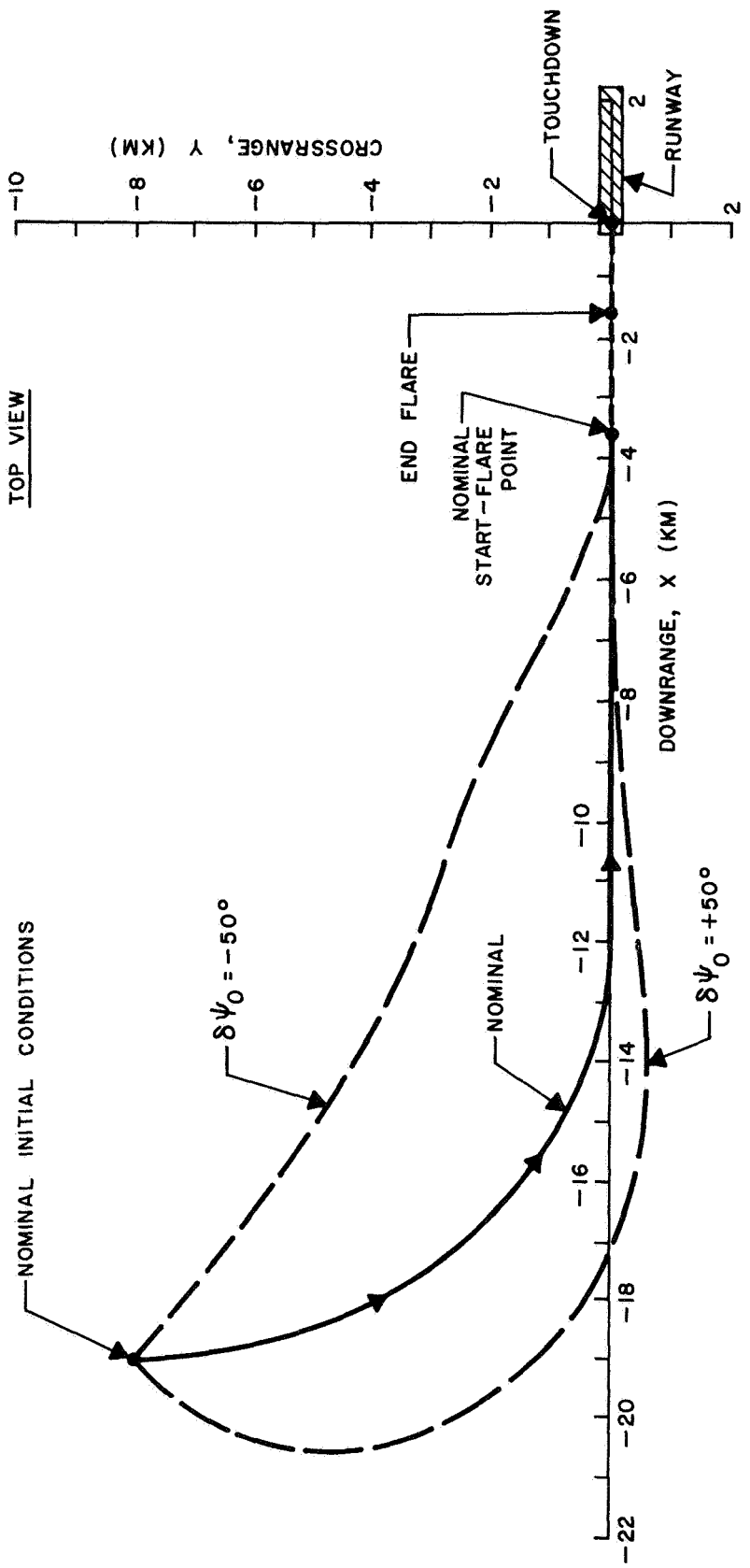

FIGURE 16. 90-DEGREE APPROACH WITH INITIAL HEADING ERRORS

TABLE VI. EFFECTS OF INDIVIDUAL INITIAL CONDITION ERRORS FOR 90-DEGREE APPROACH

Initial Condition Error	δx_f (m)	δy_f (m)	$\delta \psi_f$ (deg)	$\delta \gamma_f$ (deg)	δV_f (m/sec)
δx_o = + 3000 m	12.11	0.22	-0.17	4.45	14.12
δx_o = - 3000 m	- 26.41	0.01	0.00	-2.68	-13.49
δy_o = + 5000 m	- 17.82	0.10	-0.05	-3.34	- 5.22
δy_o = - 5000 m	- 27.14	-0.03	0.02	-3.20	-13.40
$\delta \psi_o$ = + 50 deg	- 55.37	0.03	0.00	-5.38	-26.37
$\delta \psi_o$ = - 50 deg	-115.78	-2.67	0.33	2.04	8.21
$\delta \gamma_o$ = + 6 deg	15.51	0.09	0.01	0.82	- 1.53
$\delta \gamma_o$ = - 6 deg	- 19.10	0.02	-0.02	0.78	1.17
δV_o = + 30 m/sec	- 6.78	-0.06	-0.01	1.19	3.04
δV_o = - 30 m/sec	23.43	0.07	0.00	-0.31	- 6.41

the terminal errors resulting from the initial position and heading errors discussed above, and also those arising from initial flight path angle and velocity errors of $\pm$ 6^o and $\pm$ 30 m/sec, respectively.

The guidance scheme reduces very sizable initial condition errors to very reasonable terminal errors which are well within the capability of the pilot to correct during the flare maneuver. In fact, the guidance system successfully handles errors

which are well outside the valid range of the linear perturbation approximation which was used to develop the scheme.

3.3.2 Combined Errors

To obtain an indication of the effects of combined initial condition errors, a simple linear statistical analysis was performed. If it is assumed that the system is linear for small deviations from the nominal trajectory and that there are no off-nominal disturbances acting on the vehicle during the glide (such as winds), then the errors at any altitude h are related to the errors at the initial altitude h_o by

$$\bar{y}(h) = \Phi(h,h_o)\bar{y}(h_o) \tag{40}$$

where $\bar{y}$, the state vector of the linear system, is defined as

$$\bar{y}(h) = \begin{bmatrix} \delta x(h) \\ \delta y(h) \\ \delta \psi(h) \\ \delta \gamma(h) \\ \delta V(h) \end{bmatrix} = \begin{bmatrix} x(h)-x_N(h) \\ y(h)-y_N(h) \\ \psi(h)-\psi_N(h) \\ \gamma(h)-\gamma_N(h) \\ V(h)-V_N(h) \end{bmatrix} \tag{41}$$

$\Phi(h,h_o)$ is the "state transition matrix" or "fundamental matrix," which is a function only of the initial and current altitudes.

The error covariance matrix of the system is defined as

$$C(h) = E[\bar{y}(h)\bar{y}^T(h)] \tag{42}$$

where E[ ] is the expected value of the indicated quantity. The diagonal elements of C(h) are the variances in the errors and are the squares of the standard deviations in the state variables. Substituting Equation (40) into Equation (42) and evaluating the result at the final altitude h_f, yields the terminal error covariance matrix:

$$C(h_f) = \Phi(h_f,h_o)\ C(h_o)\ \Phi^T(h_f,h_o) \tag{43}$$

Equation (43) describes the propagation of the initial condition errors to the final altitude.

The state transition matrix was evaluated for each of the nominal trajectories by the unit solution method (References 15 and 16). The results are presented below.

Straight-In Approach:

$$\Phi(h_f,h_o) = \begin{bmatrix} 0.00390 & 0.00788 & -0.0298 & 3.371 & -0.522 \\ 0.0 & -0.0000753 & -0.0106 & 0.0 & 0.0 \\ 0.0 & -0.0000141 & -0.00250 & 0.0 & 0.0 \\ 0.000613 & 0.000122 & -0.00051 & 0.0742 & 0.0877 \\ 0.00477 & -0.000633 & -0.0119 & -0.491 & 0.283 \end{bmatrix} \tag{44}$$

90-Degree Approach:

$$\Phi(h_f,h_o) = \begin{bmatrix} -0.00406 & -0.00434 & 0.127 & 2.876 & -0.726 \\ -0.0000793 & -0.0000397 & -0.00504 & -0.00763 & -0.00240 \\ -0.00000879 & -0.0000141 & -0.000738 & 0.00209 & -0.000578 \\ 0.000503 & -0.0000165 & -0.0651 & 0.129 & 0.0567 \\ 0.00464 & 0.000997 & -0.420 & -1.260 & 0.209 \end{bmatrix} \quad (45)$$

Several initial error covariance matrices were considered. The standard deviations assumed for the initial state variable errors were taken to be the same as the individual initial condition errors discussed previously (e.g., σ_x = 3000 m). Tables VII and VIII present the state variable standard deviations at the final altitude for various combinations of initial condition errors.

Comparison of the fist five rows in Tables VII and VIII with the corresponding results in Tables V and VI demonstrates the nonlinearity of the system response for such large initial errors. Further examination of Tables VII and VIII reveals that the terminal errors due to combined initial condition deviations are only slightly larger than the maximum terminal errors produced by the same individual initial deviations. It is also apparent, for example, that initial heading errors contribute the largest share of the final errors in velocity and flight path angle.

TABLE VII. EFFECTS OF COMBINED INITIAL CONDITION ERRORS FOR STRAIGHT-IN APPROACH

Initial Non-zero Standard Deviations	σ_{x_f} (m)	σ_{y_f} (m)	σ_{ψ_f} (deg)	σ_{γ_f} (deg)	σ_{V_f} (m/sec)
σ_{x_o} = 3000 m	11.70	0.00	0.00	1.84	14.3
σ_{y_o} = 5000 m	39.40	0.38	0.07	0.61	3.17
σ_{ψ_o} = 50 deg	1.49	0.53	0.13	0.03	0.59
σ_{γ_o} = 6 deg	20.20	0.00	0.00	0.45	2.94
σ_{V_o} = 30 m/sec	15.70	0.00	0.00	2.63	8.50
σ_{x_o} = 3000 m, σ_{y_o} = 5000 m	41.10	0.38	0.07	1.94	14.70
σ_{x_o} = 3000 m, σ_{y_o} = 5000 m, σ_{ψ_o} = 50 deg	41.10	0.65	0.14	1.94	14.70
σ_{γ_o} = 6 deg, σ_{V_o} = 30 m/sec	25.60	0.00	0.00	2.67	8.98
σ_{x_o} = 3000 m, σ_{y_o} = 5000 m, σ_{ψ_o} = 50 deg, σ_{γ_o} = 6 deg, σ_{V_o} = 30 m/sec	48.40	0.65	0.14	3.30	17.20

TABLE VIII. EFFECTS OF COMBINED INITIAL CONDITION ERRORS FOR 90-DEGREE APPROACH

Initial Non-zero Standard Deviations	σ_{x_f} (m)	σ_{y_f} (m)	σ_{ψ_f} (deg)	σ_{γ_f} (deg)	σ_{V_f} (m/sec)
σ_{x_o} = 3000 m	12.20	0.24	0.03	1.51	13.90
σ_{y_o} = 5000 m	21.70	0.20	0.07	0.08	4.98
σ_{ψ_o} = 50 deg	6.35	0.25	0.04	3.25	21.00
σ_{γ_o} = 6 deg	17.30	0.05	0.01	0.77	7.57
σ_{V_o} = 30 m/sec	21.80	0.07	0.02	1.70	6.26
σ_{x_o} = 3000 m, σ_{y_o} = 5000 m	24.80	0.31	0.08	1.51	14.80
σ_{x_o} = 3000 m, σ_{y_o} = 5000 m, σ_{ψ_o} = 50	25.70	0.40	0.08	3.59	25.70
σ_{γ_o} = 6 deg, σ_{V_o} = 30 m/sec	27.80	0.09	0.02	1.87	9.82
σ_{x_o} = 3000 m, σ_{y_o} = 5000 m, σ_{ψ_o} = 50 deg, σ_{γ_o} = 6 deg, σ_{V_o} = 30 m/sec	37.80	0.41	0.09	4.05	27.50

3.4 NON-STANDARD ATMOSPHERE

3.4.1 Wind Effects

The guidance scheme and the nominal trajectories were developed assuming no winds were present. Since, in general, winds will be encountered, it is of interest to determine the guidance system's performance in their presence. The effect of the winds is to alter the aerodynamic forces on the glider and, thus, push the vehicle away from the nominal trajectory.

Nine different profiles were simulated to examine their effects on each approach (see Figure 17). Four of these are constant winds, ① - ④ , four are constant shears (linear variation of wind velocity with altitude), ⑤ - ⑧ , and one is a profile which was measured at the NASA Flight Research Center, ⑨ .* Tables IX and X summarize the results of these simulations. Once again the performance of the guidance scheme is excellent. In all these cases, the disturbed trajectories were barely distinguishable from the nominals. In Figure 18, for example, the ground tracks of the straight-in approach are shown (with a much-expanded crossrange scale) for profiles ③ , ⑦ and ⑨ . Figures 19 and 20 present results for the 90^{o} approach with profiles ① , ② , ④ and ⑨ . In general, the constant shear profiles cause smaller errors throughout the descent than the

*Measured on September 2, 1966, for flight M5-12 of the M2-F2 vehicle.

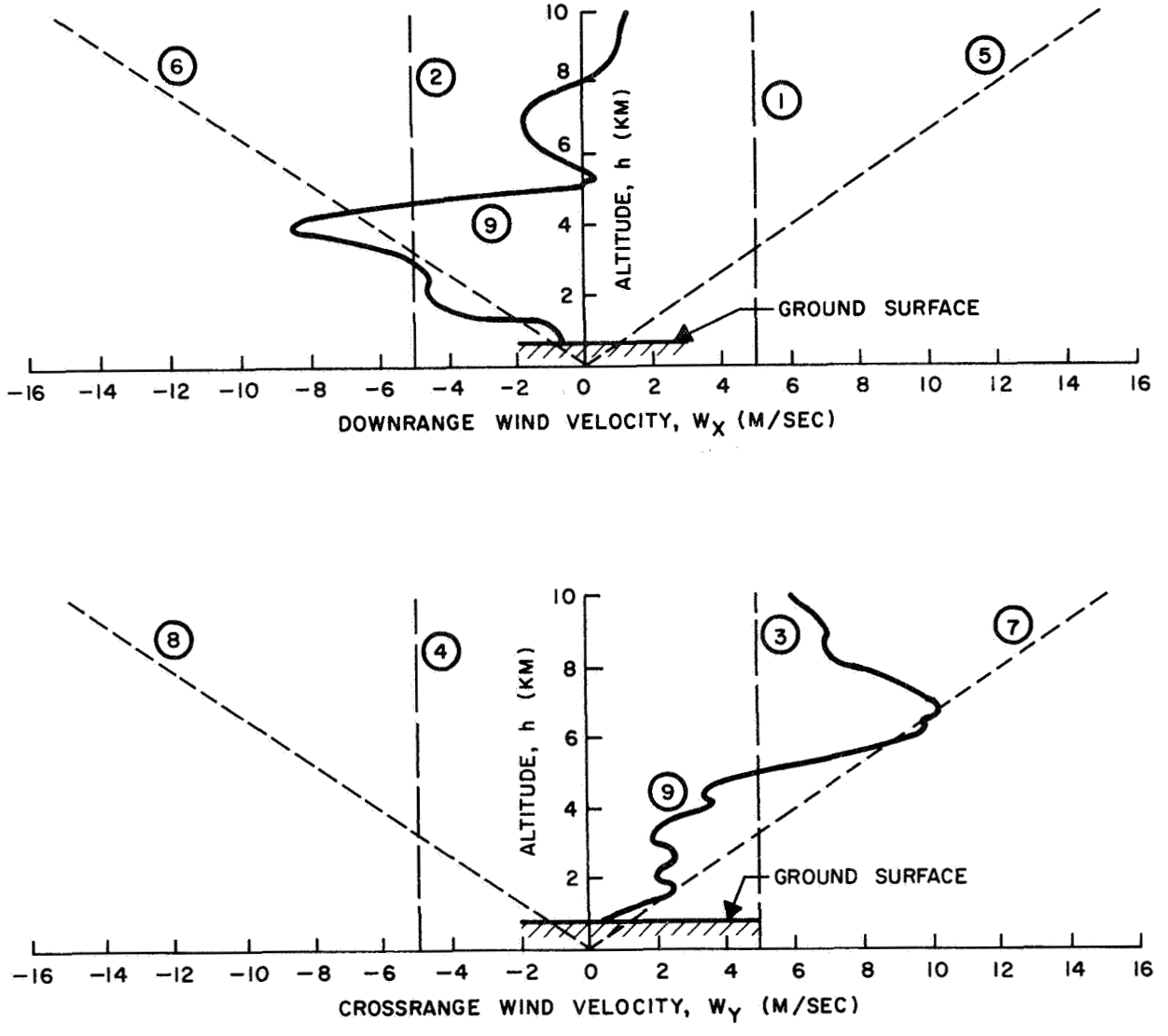

FIGURE 17. SELECTED WIND PROFILES

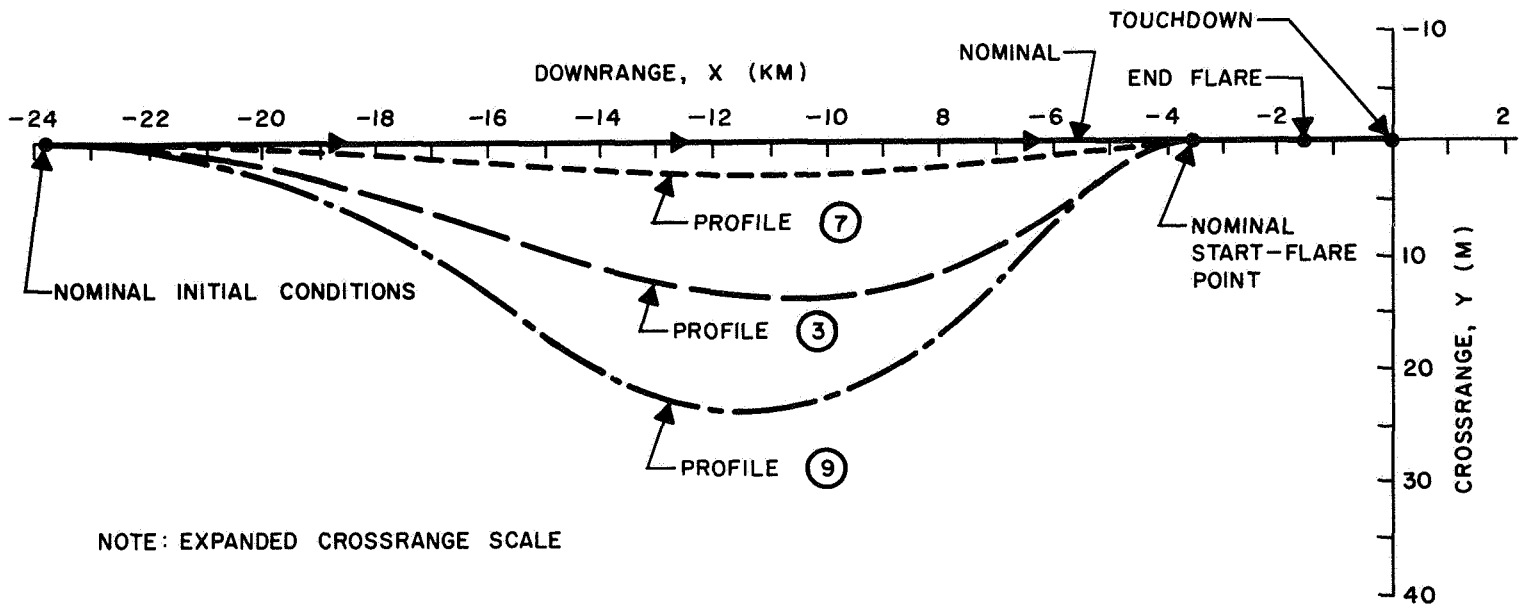

FIGURE 18. STRAIGHT-IN APPROACH WITH WIND PROFILES ③, ⑦ and ⑨

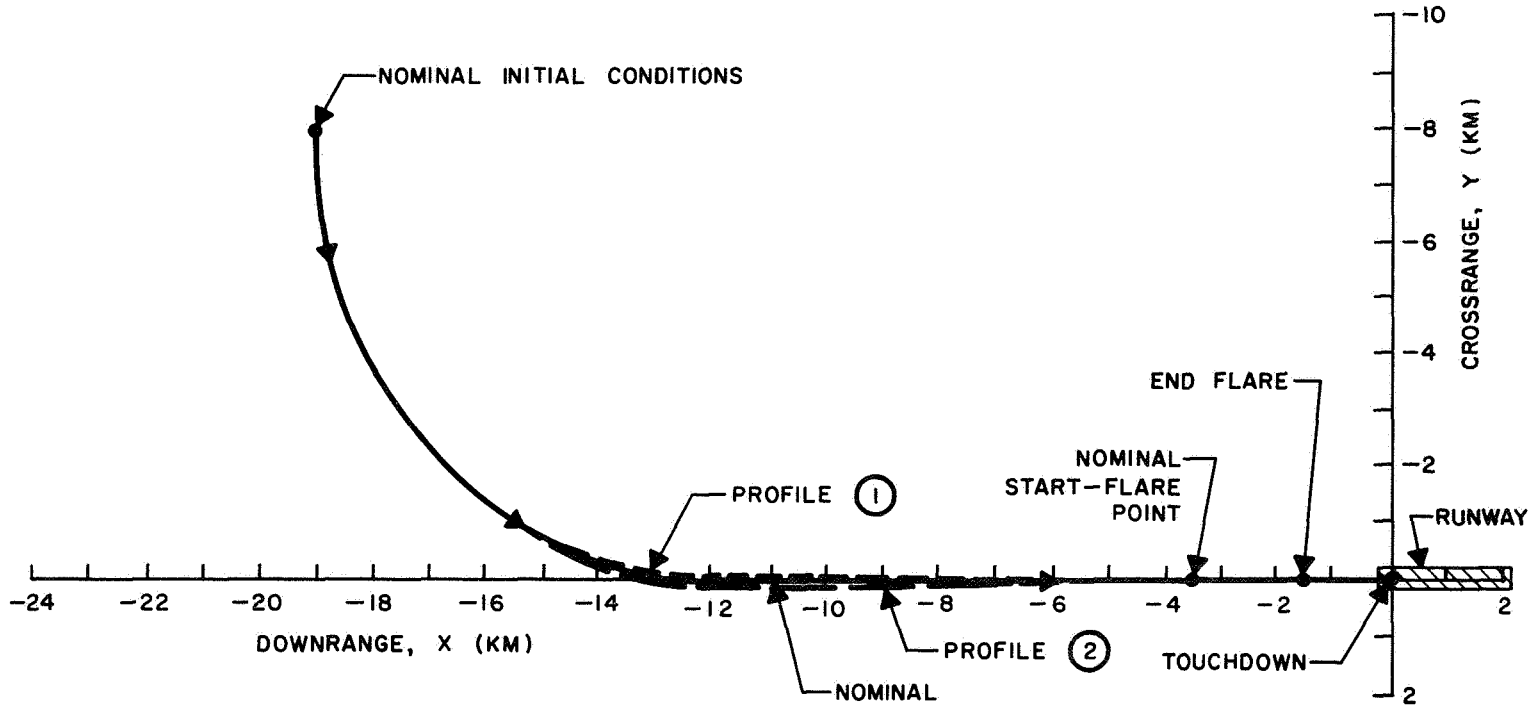

FIGURE 19. 90-DEGREE APPROACH WITH WIND PROFILES (1) and (2)

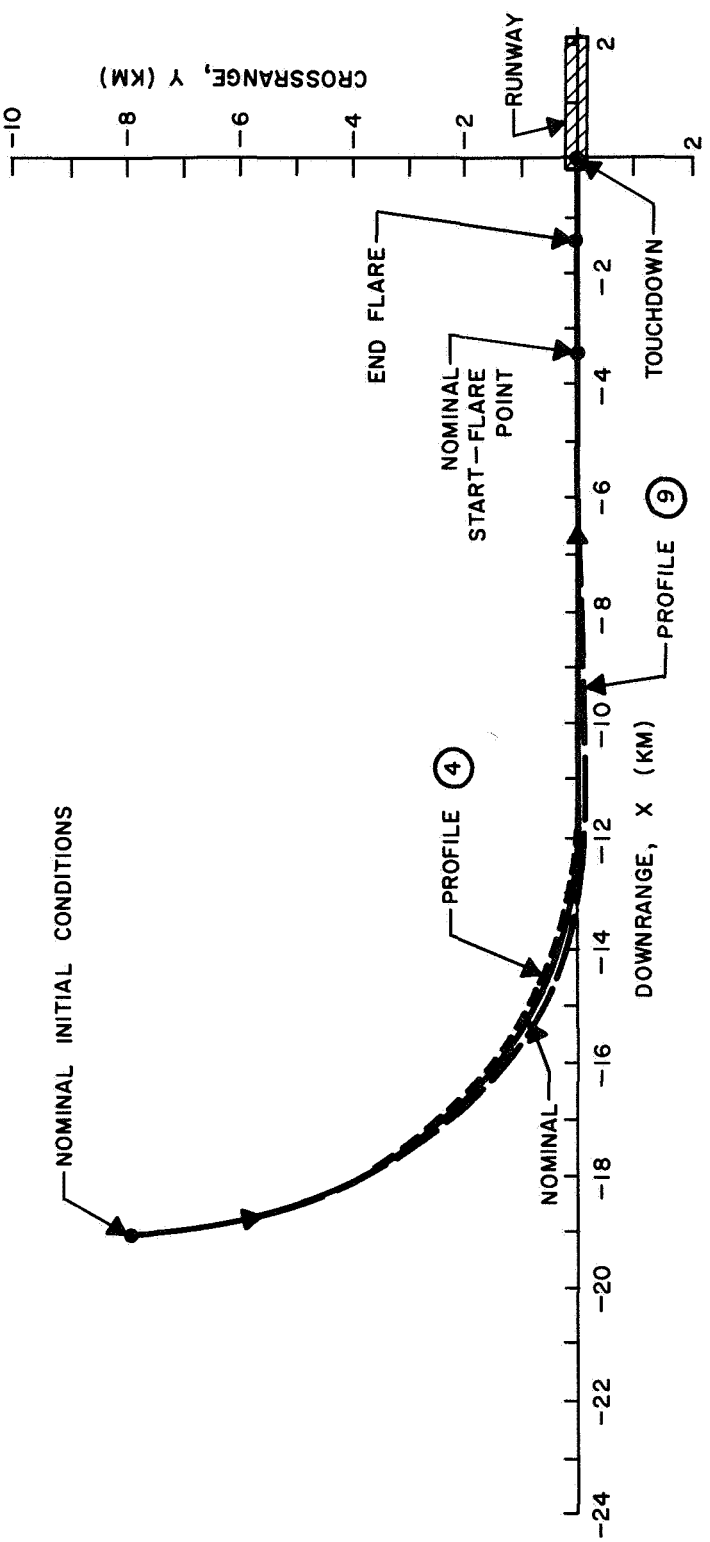

FIGURE 20. 90-DEGREE APPROACH WITH WIND PROFILES (4) and (9)

TABLE IX. WIND EFFECTS FOR STRAIGHT-IN APPROACH

Wind Profile (See Figure 17)	δx_f (m)	δy_f (m)	$\delta \psi_f$ (deg)	$\delta \gamma_f$ (deg)	δV_f (m/sec)
① W_x = + 5 m/sec	17.13	0.00	0.00	1.08	8.66
② W_x = - 5 m/sec	-16.86	0.00	0.00	-1.28	-9.14
③ W_y = + 5 m/sec	- 0.22	0.04	0.00	-0.02	-0.16
④ W_y = - 5 m/sec	- 0.22	-0.04	0.00	-0.02	-0.16
⑤ W_x' = +1.5 m/sec/km	2.80	0.00	0.00	0.18	0.88
⑥ W_x' = -1.5 m/sec/km	- 2.89	0.00	0.00	-0.18	-0.88
⑦ W_y' = +1.5 m/sec/km	0.00	0.00	0.00	0.00	-0.01
⑧ W_y' = 1.5 m/sec/km	0.00	0.00	0.00	0.00	-0.01
⑨ W_x & W_y from NASA/FRC	- 4.01	0.03	0.00	-2.10	-7.38

constant winds, even though their magnitudes are considerably greater during most of the flight.

3.4.2 Density Effects

Since the atmospheric density enters into the calculation of the feedback gains (via the parameter ℓ), and because the true atmospheric density is a random function that will always differ from the model used in obtaining the gains, simulations were run to investigate the effects of such variations on the system performance. Using Reference 17 as a guide,

TABLE X. WIND EFFECTS FOR 90-DEGREE APPROACH

Wind Profile (See Figure 17)	δx_f (m)	δy_f (m)	$\delta \psi_f$ (deg)	$\delta \gamma_f$ (deg)	δV_f (m/sec)
① W_x = + 5 m/sec	14.34	-0.12	-0.01	1.25	9.16
② W_x = - 5 m/sec	-13.38	0.00	0.01	-1.18	-9.59
③ W_y = + 5 m/sec	4.67	0.04	0.00	-0.15	-0.98
④ W_y = - 5 m/sec	- 2.15	-0.03	0.01	0.13	0.57
⑤ W'_x = +1.5 m/sec/km	1.53	-0.01	0.00	0.19	0.98
⑥ W'_x = -1.5 m/sec/km	- 1.68	0.01	0.00	-0.19	-0.99
⑦ W'_y = +1.5 m/sec/km	1.44	0.00	0.00	-0.01	-0.14
⑧ W'_y = -1.5 m/sec/km	- 1.53	0.00	0.00	0.01	0.13
⑨ W_x & W_y from NASA/FRC	19.52	0.03	0.00	-1.92	-8.94

density variations of ± 10% were selected as representing the maximum errors which might normally be encountered. The resulting trajectories are shown in Figures 21 and 22. Table XI summarizes the terminal errors which were produced by these variations. It is apparent from these results that the expected atmospheric density variations do not degrade the performance of the guidance scheme.

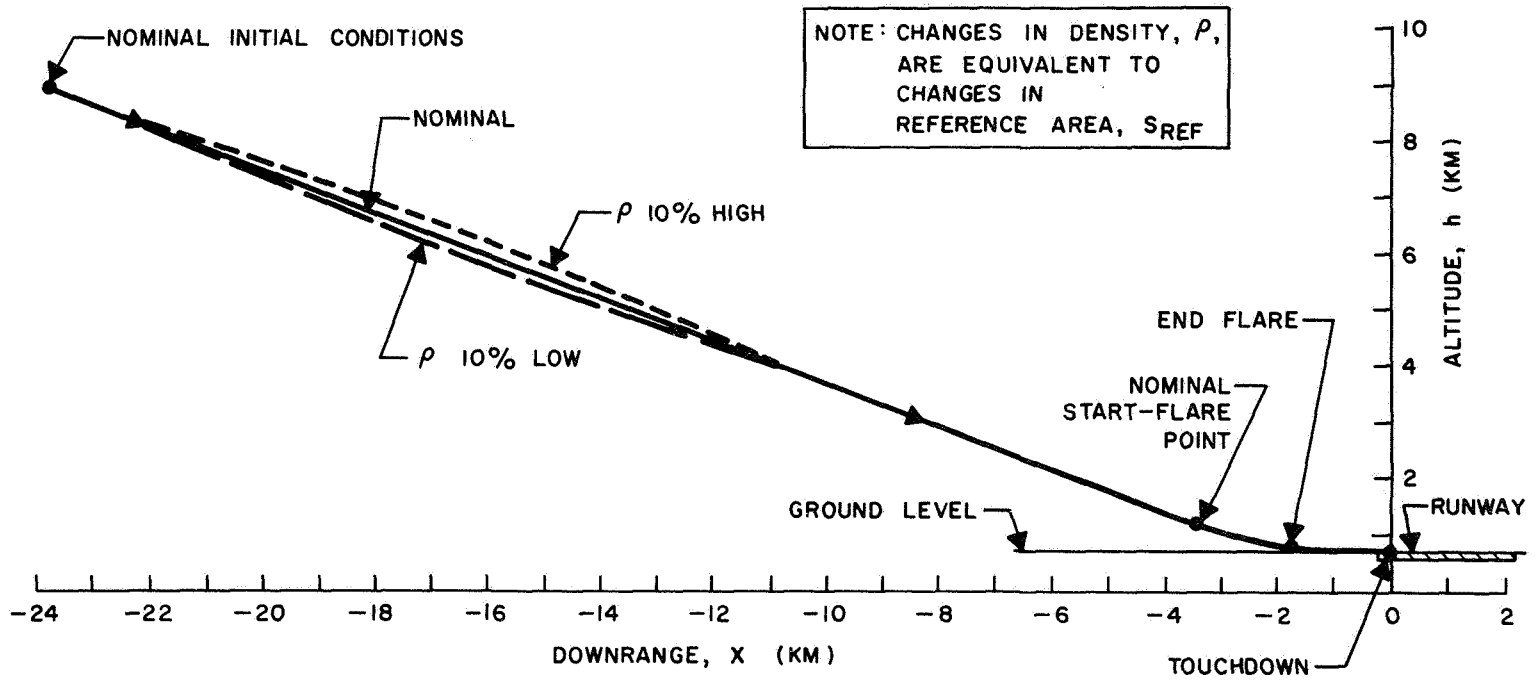

FIGURE 21. STRAIGHT-IN APPROACH WITH ATMOSPHERIC DENSITY VARIATIONS

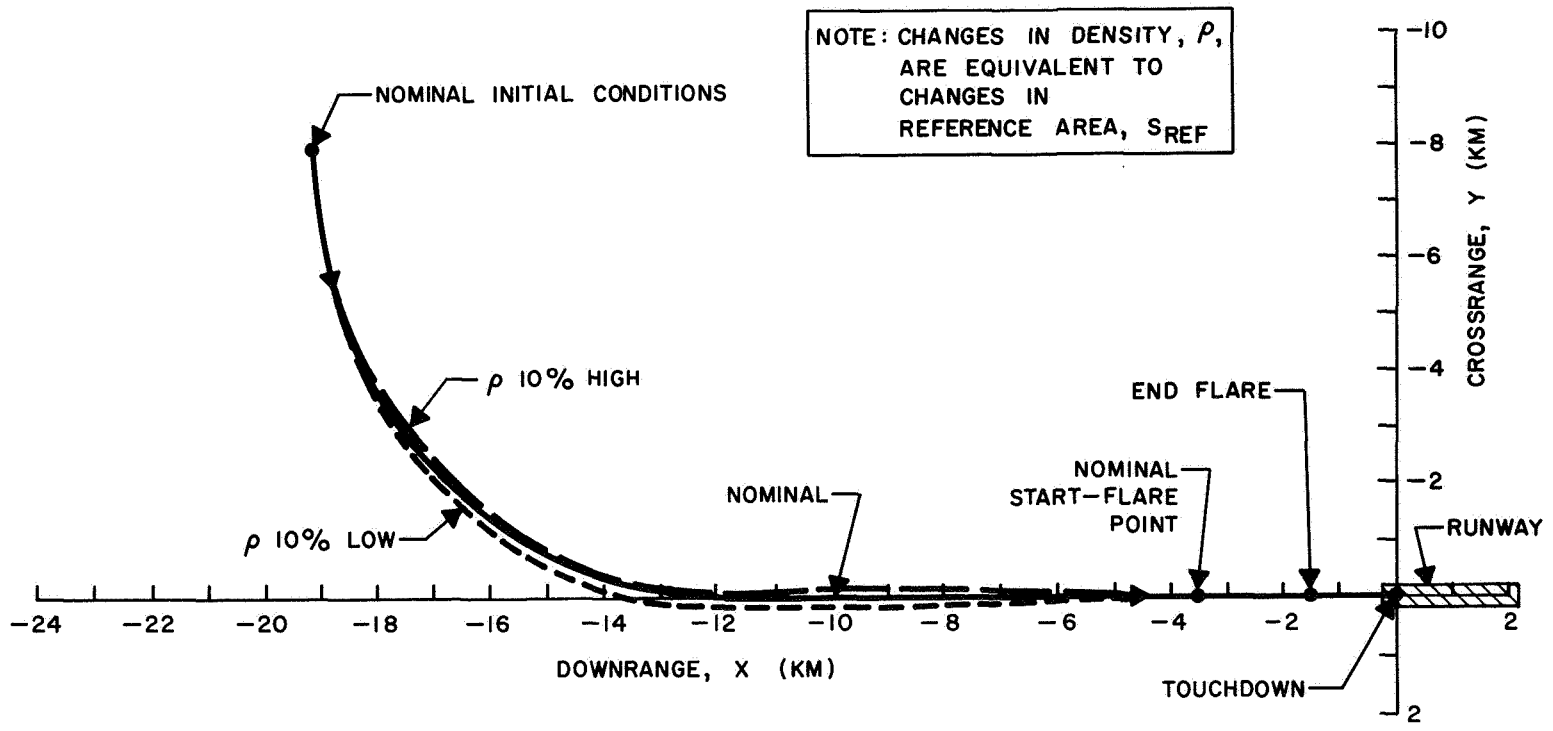

FIGURE 22. 90-DEGREE APPROACH WITH ATMOSPHERIC DENSITY VARIATIONS

TABLE XI. EFFECTS OF ATMOSPHERIC DENSITY VARIATIONS

Approach	Density Variation	δx_f (m)	δy_f (m)	$\delta \psi_f$ (deg)	$\delta \gamma_f$ (deg)	δV_f (m/sec)
Straight-In	+10%	-13.05	0.00	0.00	-0.36	-7.38
	-10%	9.69	0.00	0.00	-0.62	8.19
90-Degree	+10%	-16.80	-0.05	0.02	-0.14	-6.36
	-10%	17.95	-0.18	0.00	-0.68	6.63

3.5 OFF-NOMINAL VEHICLE CHARACTERISTICS

Another important source of errors is the uncertainty in the characteristics of the vehicle itself, primarily the mass and the aerodynamic lift and drag coefficients. The vehicle characteristics, are often not established very accurately prior to flight, and during the mission the characteristics change, mostly as a result of mass expulsion and internal mass shifts. Finally, significant changes may occur during the initial phase of entry due to ablation effects.

Since no quantitative information is available to estimate these uncertainties, it was assumed for this investigation that these characteristics could be determined to within 10% of their true values. Consequently, simulations were run with each of these parameters at ± 10% of their nominal values. The results are presented in Figures 23 to 28, and the terminal errors are summarized in Tables XII and XIII. From both the figures and the tables, it is evident that the guidance system's performance is still very good in all cases. However, the aerodynamic errors are more detrimental than equivalent uncertainties in the mass.

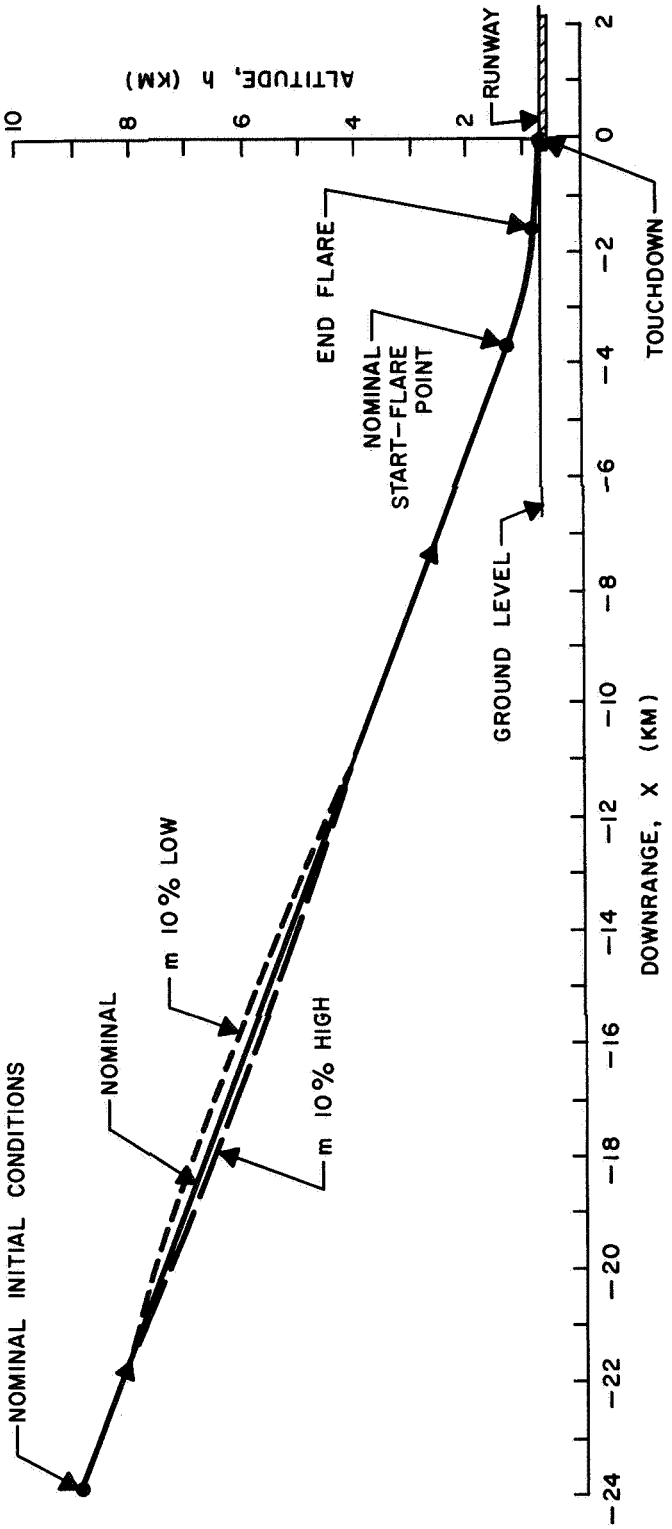

FIGURE 23. STRAIGHT-IN APPROACH WITH MASS VARIATIONS

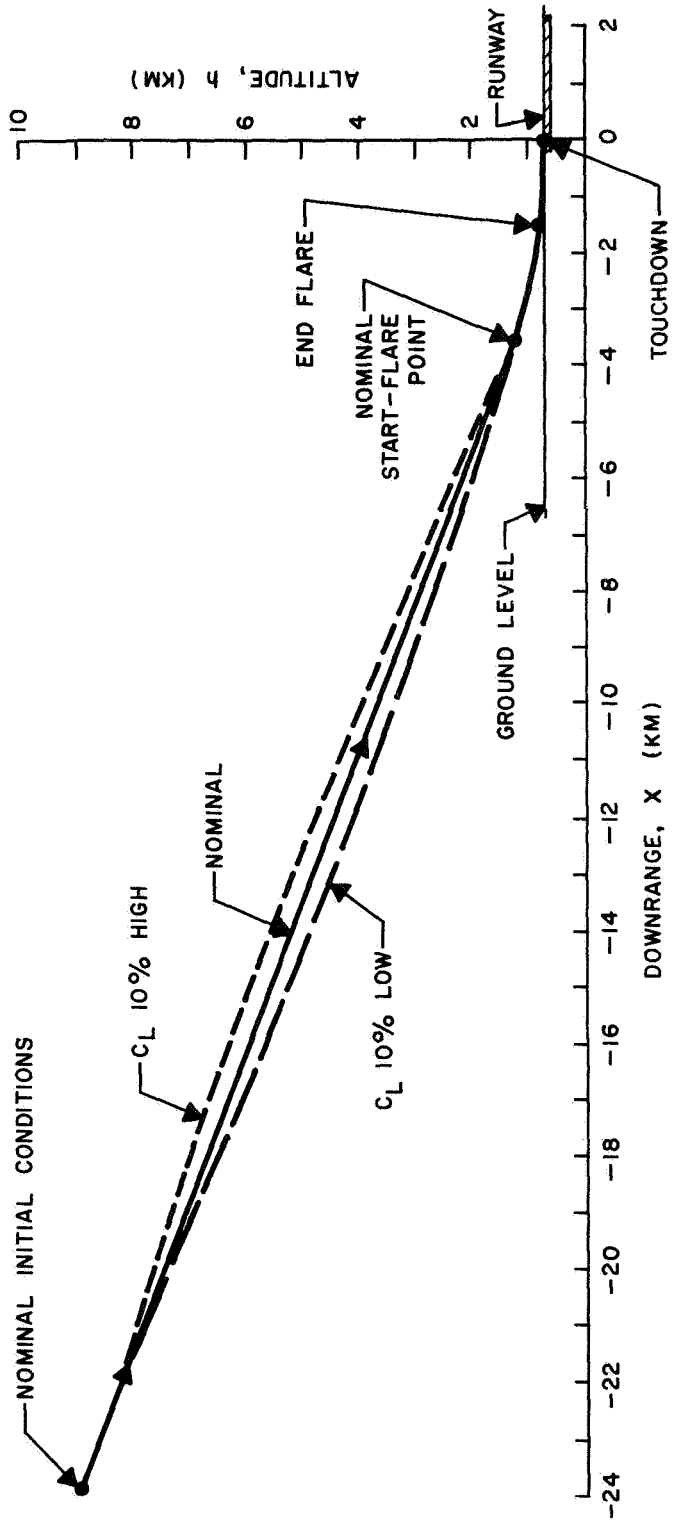

FIGURE 24. STRAIGHT-IN APPROACH WITH LIFT COEFFICIENT VARIATIONS

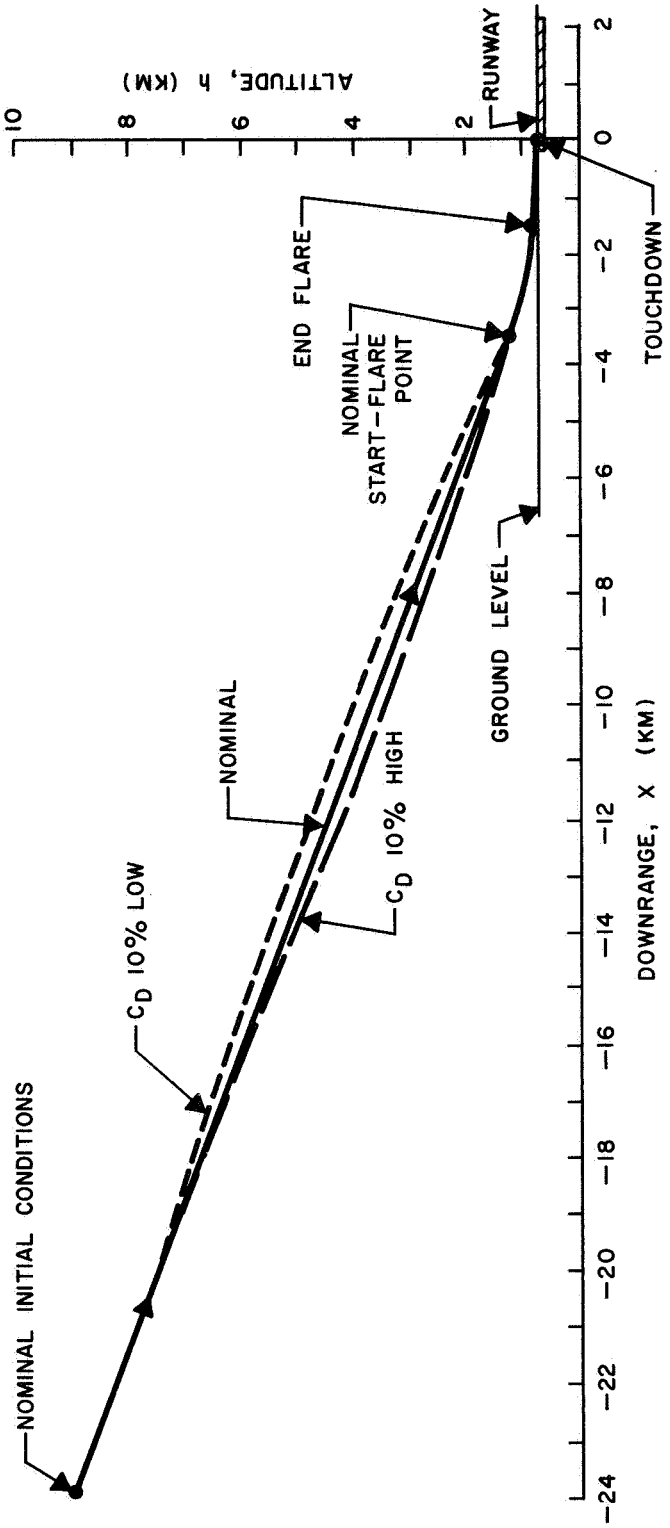

FIGURE 25. STRAIGHT-IN APPRAOCH WITH DRAG COEFFICIENT VARIATIONS

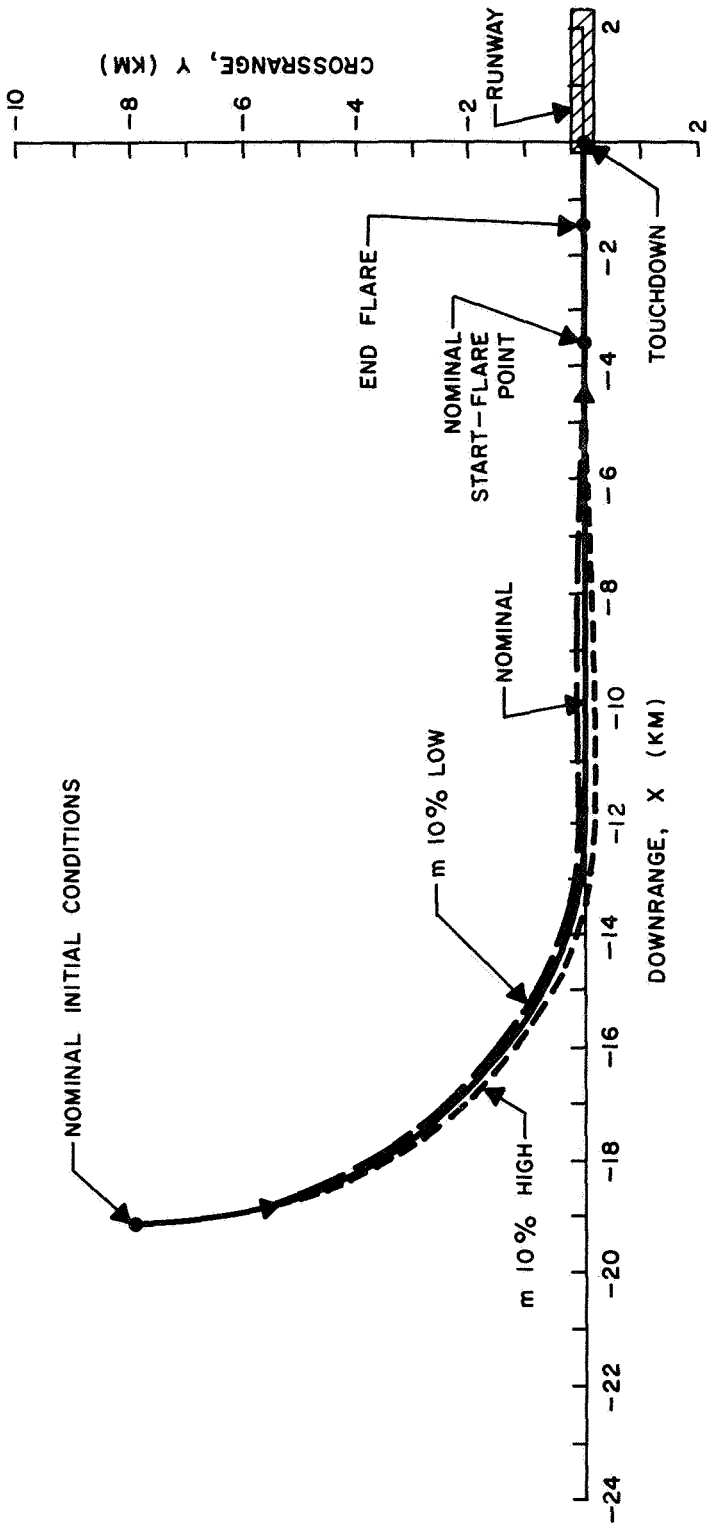

FIGURE 26. 90-DEGREE APPROACH WITH MASS VARIATIONS

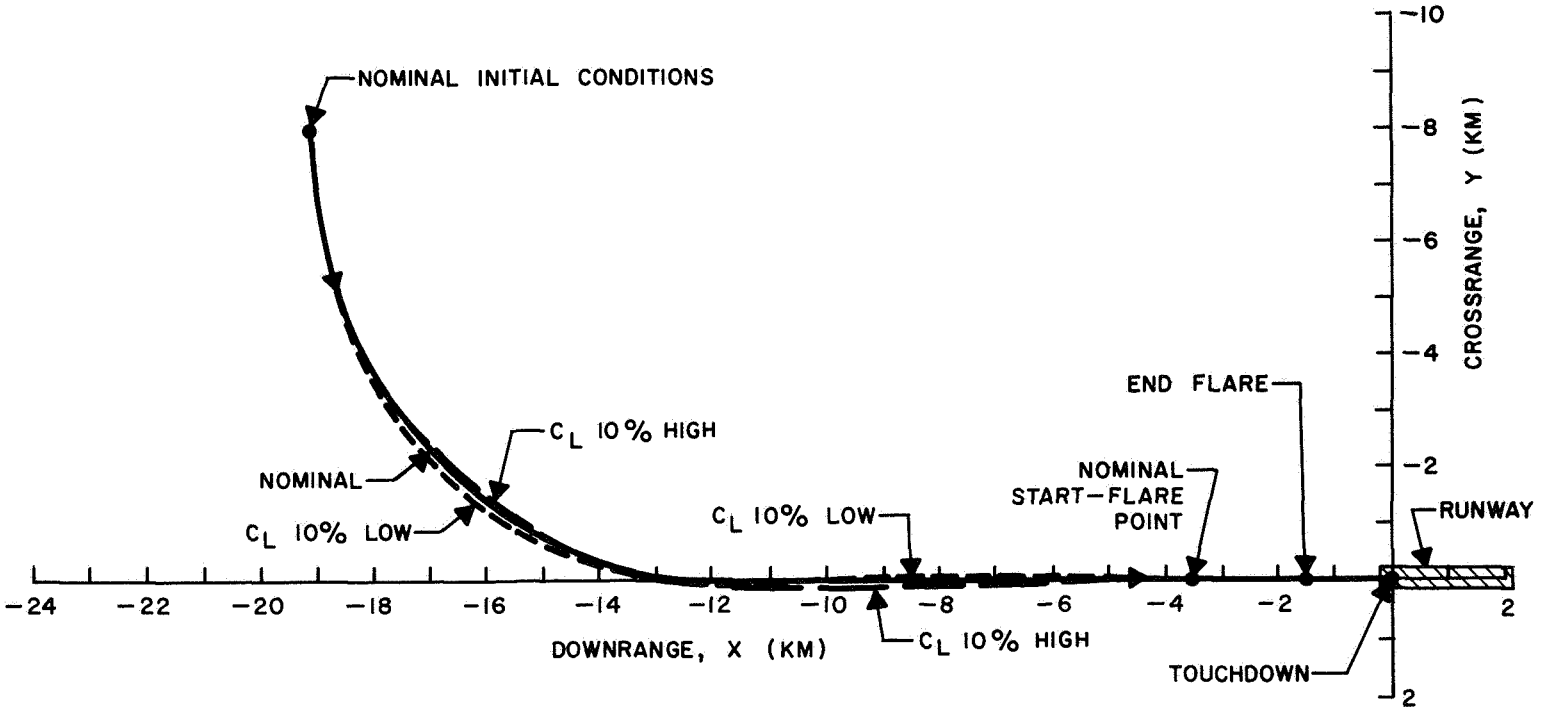

FIGURE 27. 90-DEGREE APPROACH WITH LIFT COEFFICIENT VARIATIONS

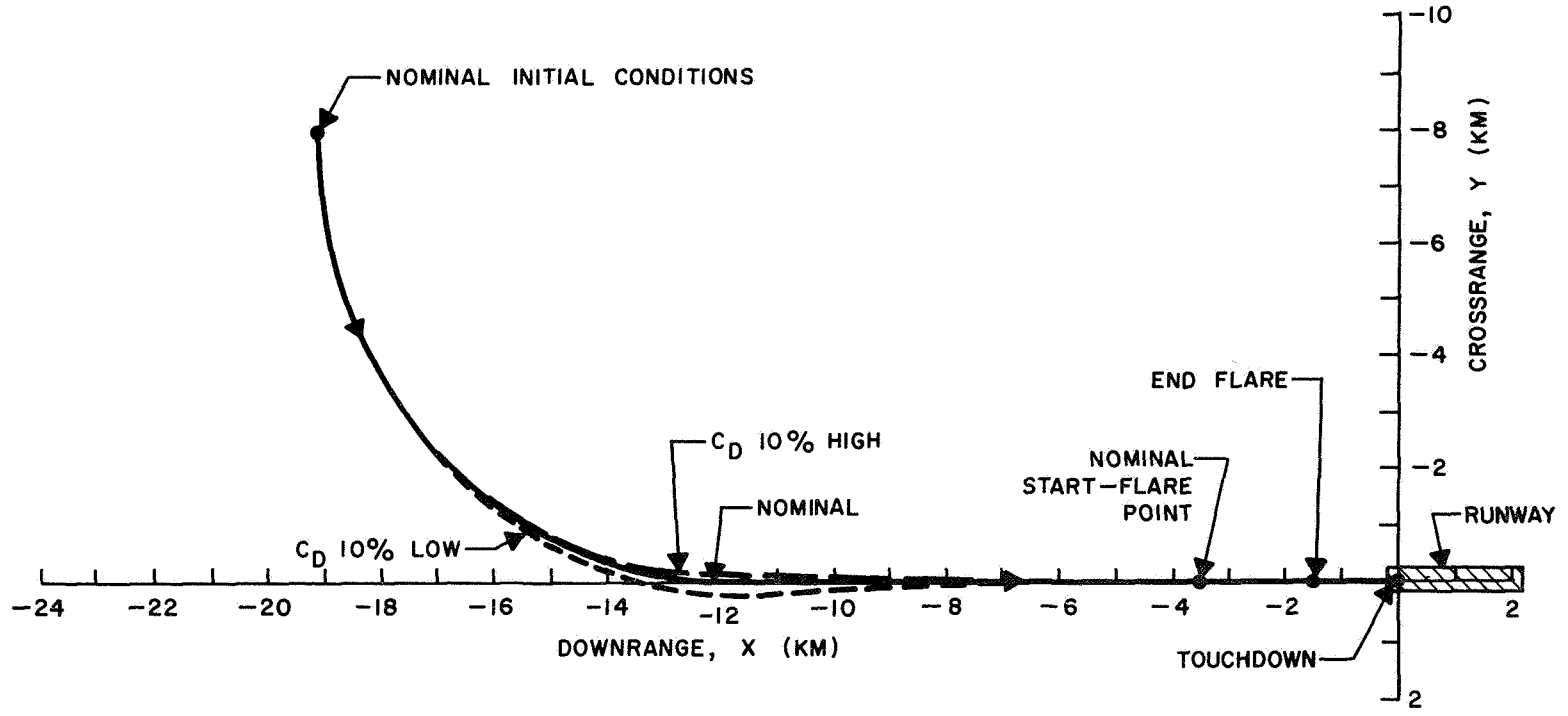

FIGURE 28. 90-DEGREE APPROACH WITH DRAG COEFFICIENT VARIATIONS

TABLE XII. EFFECTS OF OFF-NOMINAL VEHICLE CHARACTERISTICS FOR STRAIGHT-IN APPROACH

Vehicle Characteristic	Variation	δx_f (m)	δy_f (m)	$\delta \psi_f$ (deg)	$\delta \gamma_f$ (deg)	δV (m/sec)
Mass	+10%	9.45	0.00	0.00	-0.52	7.39
	-10%	-14.11	0.00	0.00	-0.45	-8.17
Lift Coefficient	+10%	39.59	0.00	0.00	5.64	10.46
	-10%	-35.11	0.00	0.00	-4.23	-14.21
Drag Coefficient	+10%	-43.26	0.00	0.00	-4.04	-20.06
	-10%	58.93	0.00	0.00	5.64	19.60

TABLE XIII. EFFECTS OF OFF-NOMINAL VEHICLE CHARACTERISTICS FOR 90-DEGREE APPROACH

Vehicle Characteristic	Variation	δx_f (m)	δy_f (m)	$\delta \psi_f$ (deg)	$\delta \gamma_f$ (deg)	δV (m/sec)
Mass	+10%	16.63	-0.16	0.00	-0.59	6.02
	-10%	-18.25	-0.07	0.02	-0.05	-7.05
Lift Coefficient	+10%	34.89	-0.04	0.10	5.78	10.93
	-10%	-44.94	0.00	0.00	-3.79	-15.27
Drag Coefficient	+10%	-47.17	0.01	0.00	-3.68	-19.48
	-10%	53.94	-0.18	0.03	5.44	19.17

Since the aerodynamic forces are directly proportional to the product of the atmospheric density and the reference area [Equations (14) and (15)], a given uncertainty in S_{ref} has the same effect on the performance as an identical, but separate, fixed percentage deviation in ρ. Comparing Table XI with Tables XII and XIII, a 10% change in density produces a 10% change in both lift and drag, but this has less effect on the terminal accuracy than a 10% change in either the lift or the drag individually. Thus, the scheme is more sensitive to uncertainties in (L/D) than it is to errors in the total aerodynamic force.

SECTION IV

CONCLUSIONS AND RECOMMENDATIONS

4.1 SUMMARY OF CONCLUSIONS

A simple perturbation feedback scheme has been developed for terminal guidance of manned lifting entry vehicles. The point-mass equations of motion were simplified and linearized about a nominal trajectory and the quadratic synthesis technique was utilized to obtain a linear feedback law for the simplified system. This law was then applied to the original system. A digital simulation of the M-2 lifting entry vehicle was used to evaluate the performance of the guidance scheme for a variety of off-nominal conditions. The results of the study are summarized below:

1. It was observed that the velocity and flight path angle of current lifting body configurations approach a quasi-steady condition during the terminal phase of flight. By neglecting the rate of change of these quantities and by using altitude rather than time as the independent variable, the number of state variables describing the system was reduced to three, the two position coordinates in the horizontal plane and the heading angle.

2. The equations of the reduced system were linearized about a nominal trajectory. A performance index was then selected which was quadratic in both the terminal

state variable errors and in the control variable deviations. The minimization of this performance index yielded a linear feedback guidance law [Equation (38)], with the feedback gains being functions of altitude (quadratic synthesis).

3. The terminal guidance scheme can be easily implemented. The feedback gains are pre-calculated for a selected nominal trajectory and stored as functions of altitude in the airborne computer, along with the nominal state and control variable histories. During flight, the state variables would be estimated from measurements and their deviations from nominal would be used to compute corrections to the nominal control histories. The computational and storage requirements are very modest, so that the values for several nominal approaches could be carried along for contingencies and for greater flexibility.

4. The scheme described herein provides very precise terminal guidance for extremely large initial condition errors. It successfully handles errors which are well outside the linear range of operation assumed in its development. The errors remaining at the beginning of flare are well within the pilot's capability of correcting during the final flare and landing maneuvers.

5. A linear statistical analysis of the effects of combined initial condition errors indicates that the resulting terminal errors are not significantly larger than the largest errors produced by the corresponding individual initial condition perturbations.

6. The guidance scheme performed very well in the presence of several wind profiles. Steady winds parallel to the runway, either in the landing direction or opposed to it, produced the largest terminal errors, but even these were very acceptable.

7. Atmospheric density variations of ± 10% resulted in very small terminal errors, which were all well within the acceptable limits.

8. Uncertainties of ± 10% in the knowledge of the vehicle's mass or aerodynamic forces produced only minor errors at the final altitude.

9. Errors of ± 10% in the lift or drag coefficient (separately) resulted in terminal errors which were somewhat larger but still acceptable. Since the lift over drag ratio (L/D) is unaffected by changing both lift and drag by the same amount or by the atmospheric density, but is altered by separate changes in either the lift or the drag, these results indicate the guidance scheme is more sensitive to

uncertainties in L/D than it is to uncertainties in the total aerodynamic force.

4.2 SUGGESTIONS FOR FURTHER RESEARCH

Further examination of the following items would help to establish the capabilities and requirements of the proposed terminal guidance scheme:

1. The present investigation was limited to subsonic flight. However, to be of practical value, a terminal guidance scheme must be capable of operating well into the supersonic flight regime. Since it is unlikely that the quasi-equilibrium glide assumption will be useful during transonic and supersonic flight, it will probably be necessary to increase the dimension of the system to four or five state variables. In this event, it might be advantageous to employ the "energy-state" approximation (see Reference 18) to reduce the system complexity. The energy-state concept might also be useful in designing nominal trajectories which provide nearly optimum performance (such as maximum crossrange). The resulting guidance scheme should be evaluated to determine its performance with off-nominal initial conditions, winds, nonstandard atmosphere, etc.

2. A more complete statistical analysis of the guidance scheme's performance would be valuable in assessing the

combined effects of all likely off-nominal conditions, including initial conditions, vehicle characteristics, winds and atmospheric density. In order to conserve both computation and data reduction time, a linear stochastic analysis would be used. (However, a limited Monte Carlo study would also be useful to evaluate the importance of nonlinear effects.) The stochastic behavior of the state and control vector perturbations would be found by examining the behavior of their respective error covariance matrices. A further improvement, at little additional complexity, would be to include the effects of measurement uncertainties in the analysis. Realistic estimates of the expected measurement uncertainties could be obtained for available sensors. These would then be incorporated into the propagation of the error covariance matrices. Either continuous or sampled measurements could be considered.

3. To provide rapid and accurate implementation of the angle of attack and bank angle commands, an attitude control system should be designed for use with the terminal guidance scheme. The time-domain quadratic synthesis technique could be used to calculate the feedback gains at various points along the nominal trajectory. The configuration selected should assume

decoupled longitudinal and lateral-directional rigid-body motions, and not require a mechanical rudder-aileron interconnect. Such a scheme would use the aerodynamic controls in the most effective manner for controlling short-period disturbances and for responding to guidance commands. This system could then be combined with the terminal guidance scheme in a full six degree-of-freedom simulation, and the overall effectiveness could be examined in the presence of off-nominal initial conditions, winds, gusts, etc.

4. In order to demonstrate the versatility of the terminal guidance scheme, it should be applied to vehicles other than the M-2 lifting body entry vehicle. Reliable data could be obtained for the other two existing lifting bodies (H1-10 and X-24A) and studies parallel to those conducted under the present contract could be performed for these vehicles. Other interesting applications would be to a typical V/STOL aircraft, such as the tilt-wing XC-142, or to a supersonic transport (SST). This task would require obtaining and programming the vehicle data (physical, aerodynamic, engine), deriving a suitable model for the aircraft, and selecting a satisfactory nominal trajectory. A simple straight-in approach should be considered first, with angle of attack and wing tilt

angle (V/STOL) or throttle setting (SST) as the control variables. Maneuvering approaches in which the bank angle is an additional control variable could be examined later. The effectiveness of the system for providing accurate landing in the presence of initial errors, winds, etc., could then be evaluated as in the present study.

5. A computer sizing study would provide useful data for estimating the onboard computer requirements of the guidance scheme. Trade-off studies should be conducted to determine the effects on the system's performance of such factors as: the number and choice of altitudes at which the feedback gains are stored; the discretization levels of both the state variable measurements and the guidance commands; the word length used in the calculations; and the sampling frequency for updating the measurements and commands. The number of nominal approach trajectories and associated feedback gains which might reasonably be carried along on a mission should be examined as well. Consideration should also be given to the possibility of manual implementation of the guidance commands by means of a visual display to the pilot. Finally, a preliminary estimate of the necessary onboard computer specifications should be drawn from the results obtained.

REFERENCES

1. Wingrove, R. C., "Survey of Atmosphere Re-entry Guidance and Control Methods," AIAA Journal, Vol. 1, No. 9, September 1963.

2. Lessing, H. C., Tunnell, P. J. and Coate, R. E., "Lunar Landing and Long Range Earth Re-entry Guidance by Application of Perturbation Theory," AIAA Journal of Spacecraft, Vol. 1, No. 2, March-April 1964.

3. Perlmutter, L. D. and Carter, J. P., "Reference Trajectory Re-entry Guidance Without Pre-Launch Data Storage," AIAA Preprint No. 65-48, AIAA Second Aerospace Sciences Meeting, New York, N. Y., January 1965.

4. Holleman, E. C. and Adkins, E. J., "Contributions of the X-15 Program to Lifting Entry Technology," AIAA Journal of Aircraft, Vol. 1, No. 6, November-December 1964.

5. Thompson, M. O., "Progress Report on the Manned Lifting-Body Flight Test Program," AIAA Paper No. 66-838, AIAA Third Annual Meeting, Boston, Massachusetts, November 1966.

6. Zvara, J., Mikami, K. and Thompson, J. H., A Study of the Terminal Trajectory Dynamics for the M-2 and HL-10 Lifting-Body Vehicles (U), NASA CR-73081, Kaman AviDyne TR-42, Kaman AviDyne, Burlington, Massachusetts, April 1967 (CONFIDENTIAL).

7. Zvara, J., et al, Six-Degree-of-Freedom Analysis of Lifting Re-entry Vehicle Terminal Landing, Volume I. Interim Scientific Report (U), Kaman AviDyne TR-45, Kaman AviDyne, Burlington, Massachusetts, June 1967 (CONFIDENTIAL).

8. Horton, V. W., Eldredge, R. C. and Klein, R. E., Flight-Determined Low-Speed Lift and Drag Characteristics of the Lightweight M2-F1 Lifting Body, NASA TN D-3022, September 1965.

9. Smith, H. J., Evaluation of the Lateral-Directional Stability and Control Characteristics of the Lightweight M2-F1 Lifting Body at Low Speeds, NASA TN D-3022, September 1965.

10. Mort, K. W. and Gamse, B., Full-Scale Wind Tunnel Investigation of the Longitudinal Aerodynamic Characteristics of the M2-F1 Lifting Body Flight Vehicle, NASA TN D-3330, March 1966.

11. Anon., M2-F2 Full-Scale Flight Vehicle Wind-Tunnel Data From NASA Flight Research Center (U), Edwards Air Force Base, California (CONFIDENTIAL).

12. Anon., M2-F2 Aerodynamic Summary Data From NASA Flight Research Center (U), Edwards Air Force Base, California (CONFIDENTIAL).

13. Rainey, R. W., Summary of Advanced Manned Lifting Entry Vehicle Study (U), NASA TM X-1159, October 1965 (CONFIDENTIAL).

14. Anon, U.S. Standard Atmosphere, 1962, U S. Government Printing Office, Washington D.C., December 1962.

15. Bryson, A. E. and Ho, Y. C., Applied Optimal Control Blaisdell Co., Waltham, Massachusetts, 1968.

16. Schwarz, R. J. and Friedland, B., Linear Systems, McGraw-Hill Co., Inc., New York, 1965.

17. Anon., U. S. Standard Atmosphere Supplements, 1966, U. S. Government Printing Office, Washington, D. C., 1966.

18. Bryson, A. E., Jr., Desai, M. N. and Hoffman, W. C., The Energy-State Approximation in Performance Optimization of Supersonic Aircraft, AIAA Paper No. 68-877, AIAA Guidance, Control and Flight Dynamics Conference, Pasadena, California, August 1968.